Resource Allocation in UAV-Enabled Wireless-Powered MEC Networks With Hybrid Passive and Active Communications

Qian Li, Liqin Shi, Zhongjun Zhang, and Gan Zheng, *Fellow, IEEE*

***Abstract*—This article proposes a novel unmanned aerial vehicle (UAV)-enabled wireless-powered mobile edge computing (WP-MEC) network, where several Internet of Things (IoT) nodes use the energy harvested from the UAV's radio frequency signals to support the local computation and the hybrid active–passive communications-based task offloading. Two weighted sum computation bits (WSCB) maximization problems are formulated under the partial and binary offloading, respectively, by jointly optimizing the local computing frequencies and time, the IoT nodes' reflection coefficients, the IoT nodes' transmit powers, the UAV's trajectory, etc., subject to the quality-of-service and energy-causality constraints per IoT node, the speed constraint of the UAV, etc. Since the formulated problems are highly nonconvex, two iterative algorithms are proposed to solve the formulated problems under two modes. Simulation results demonstrate that the proposed iterative algorithms have a fast convergence rate, and the proposed schemes achieve higher WSCB than several baseline schemes.**

***Index Terms*—Computation bits, hybrid active–passive communications, unmanned aerial vehicle (UAV)-enabled wireless-powered mobile edge computing (WP-MEC).**

I. Introduction

IT HAS been witnessed that the Internet of Things (IoT) plays a significant role in future applications by deploying massive IoT nodes to provide intelligent services. However, owing to the production cost limitation, IoT nodes are usually energy- and computation-constrained, bringing many challenges in realizing IoT nodes-based intelligent services. One of major challenges is how to timely process the computation-intensive tasks at IoT nodes while reducing or even avoiding energy consumption of their batteries [1]. Wireless-powered mobile edge computing (WP-MEC), which seamlessly integrates wireless power transfer (WPT) [2] and mobile edge computing (MEC) [3], [4] as a whole, has been proposed as an efficient solution to address this challenge. The key idea of WP-MEC is to let IoT nodes harvest energy from radio frequency (RF) signals of a dedicated energy source, and use their harvested energy to support the data offloading and task computation under the binary or partial computation offloading [1], [5]. Accordingly, the energy harvesting (EH), data computation, and offloading are coupled with each other, which calls for new optimization frameworks.

You et al. [5] proposed a WP-MEC network with a single IoT node, and focused on maximizing the successful computation probability under a binary offloading mode, subject to the energy-causality and delay constraints. Considering a WP-MEC network with multiple IoT nodes, Huang et al. [6] maximized the weighted sum-computation rate maximization by optimizing the binary computation offloading decision, the EH time, and the offloading time per IoT node. In [7], the total energy consumption at all IoT nodes and the power beacon (PB) was minimized under a partial offloading mode, while satisfying the minimal required computation bits, delay, and energy-causality constraints per IoT node. Mao et al. [8], Ji and Guo [9], Shi et al. [10], and Zhou et al. [11] introduced the computation energy efficiency (CEE) that is calculated as the ratio of the computed task bits to the corresponding consumed energy, and designed various optimization frameworks for WP-MEC networks.

In the above works [5], [6], [7], [8], [9], [10], [11], the task data are offloaded to the MEC server via active communications (ACs) that require power-consuming components, e.g., oscillators and analog-to-digital/digital-to-analog converters. Owing to the use of high power-consuming components and the low efficiency of EH, more time will be allocated to the EH at each IoT node, leaving less time for data offloading and limiting the performance of data offloading in WP-MEC. Different from AC, the backscatter communication (BackCom), one of low power-consuming passive communications, enjoys a lower power consumption and a lower offloading rate than AC by allowing an IoT node to modulate and reflect the incident signals for task offloading [12]. In order to achieve efficient task offloading, BackCom has been integrated into WP-MEC to form WP-MEC with hybrid active–passive communications [13], where the advantages of hybrid active–passive communications can be fully exploited. Recent works [14], [15], [16], [17], [18], [19] have validated the advantages of WP-MEC via hybrid active–passive communications over the WP-MEC via AC in terms of the computation

Manuscript received 30 May 2022; revised 24 September 2022; accepted 9 October 2022. Date of publication 14 October 2022; date of current version 24 January 2023. This work was supported in part by Scientific Research Program Funded by Shaanxi Provincial Education Department under Grant 22JK0570; in part by the China Railway First Survey and Design Institute Group Company Ltd., Research Program under Grant 2022KY52ZD(ZNXT)-03; and in part by the National Natural Science Foundation of China under Grant 62201451 and Grant 62071352. *(Corresponding author: Liqin Shi.)*

Qian Li and Zhongjun Zhang are with the School of Computer Science and Technology, Zhoukou Normal University, Zhoukou 466001, China.

Liqin Shi is with the Shaanxi Key Laboratory of Information Communication Network and Security, Xi'an University of Posts and Telecommunications, Xi'an 710121, China (e-mail: liqinshi@hotmail.com).

Gan Zheng is with the School of Engineering, University of Warwick, CV4 7AL Coventry, U.K. (e-mail: gan.zheng@warwick.ac.uk).

Digital Object Identifier 10.1109/JIOT.2022.3214539

bits, CEE, and computation delay. However, it was assumed in the existing works [14], [15], [16], [17], [18], [19] that the location of the dedicated energy source is fixed. In such a case, the harvested energy of each IoT node is constrained by the distance from the dedicated energy source to the IoT node, and this calls for a mobile energy source to replace the fixed one, in order to make full use of the mobility of the energy source for increasing the harvested energy per IoT node. Recently, the unmanned aerial vehicle (UAV) has been considered as a mobile energy/signal source in multiple wireless communication networks, i.e., relaying communication systems [20], intelligent reflecting surface (IRS)-assisted wireless networks [21], WP-MEC networks [22], [23], [24], [25], [26], etc. For example, in [20], the UAV was adopted as a relay to help transmit information and the minimum average secrecy rate among all users was maximized for UAV-relaying systems with local caching. In IRS-assisted UAV networks, the UAV served as a mobile signal source and the secure communication between the UAV and the legitimate user was guaranteed [21]. In UAV-enabled WP-MEC, the UAV is deployed as a mobile energy source for charging IoT nodes via Line-of-Sight (LoS) links and various resource allocation schemes have been proposed to achieve different optimization goals [22], [23], [24], [25], [26]. We note that the previous works [22], [23], [24], [25], [26] on UAV-enabled WP-MEC only considered the AC for data offloading, while the data offloading via hybrid active–passive communications has not been exploited. This motivates us to configure a new UAV-enabled WP-MEC network to make full use of the advantages of hybrid active–passive communication-based offloading.

In this work, we employ the hybrid active–passive communication in UAV-enabled WP-MEC for realizing more efficient data offloading, and propose to maximize the weighted sum computation bits (WSCB) of all IoT nodes. To the authors' best knowledge, this is the first work that studies the resource allocation problems for the UAV-enabled WP-MEC network with hybrid active–passive communications. Our main contributions are listed as follows.

1) We propose a novel UAV-enabled WP-MEC network, in which a UAV is dispatched as a mobile energy source that provides energy to all IoT nodes and all IoT nodes take turns to perform hybrid active–passive communications-based data offloading by fully exploiting the incident signals transmitted by the UAV.
2) Considering the partial and binary offloading modes, we formulate two WSCB maximization problems, by optimizing multiple optimization variables, i.e., the IoT nodes' local computation frequencies and time, reflection coefficients and the transmit power of the IoT nodes, the UAV's trajectory, etc. In order to solve them, we first obtain the closed-form expression of the optimal computing time for the IoT node who performs local computation under two modes based on the proof by contradiction. Then for the partial offloading, we propose a two-stage alternating iterative algorithm to solve the formulated optimization problem and derive the closed-form expressions for the optimal local computing frequencies and time, the optimal power reflection coefficients and the optimal transmit powers at IoT nodes under any given trajectories. For the binary offloading, in order to solve the formulated mixed-integer optimization problem, we propose a three-stage alternating iterative algorithm to obtain the IoT nodes' local computation frequencies and time, the reflection coefficients, the UAV's trajectory, the mode selection per IoT node for choosing either task offloading or local computation, etc.
3) Simulation results validate the fast convergence of the proposed iterative algorithms and demonstrate that the superiorities of the proposed schemes in terms of WSCB.

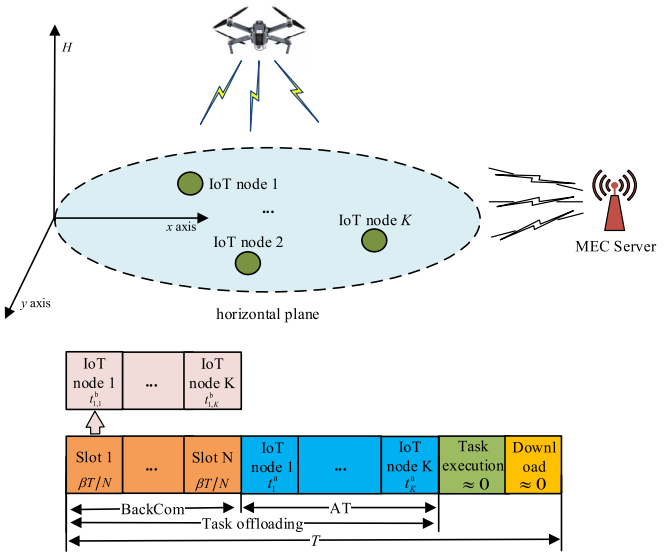

Fig. 1. UAV-enabled WP-MEC network with hybrid passive and ACs and its frame structure.

II. System Model

A UAV-enabled WP-MEC network with hybrid passive and ACs is considered, as shown in Fig. 1, where a UAV provides energy signals to K single-antenna IoT nodes and a MEC server is deployed to provide MEC services for these IoT nodes. Specifically, the IoT nodes should harvest energy from the RF signals of the UAV and then offload their task bits to the MEC server for computation by means of the combination of BackCom and AC, namely, hybrid passive and ACs, and/or perform local computing by using its harvested energy. Suppose that each IoT node is energy constrained and each IoT node only uses its harvested energy to perform task offloading and/or local computation. In order to realize tasks offloading and computing, all IoT nodes should be equipped with four separate circuits which are the energy harvester, the computing circuit, the backscatter circuit, and the AC circuit, respectively. Accordingly, each IoT node can offload tasks when performing local computation.

Assume that the location of the kth ($k \in \mathcal{K} = \{1, 2, \ldots, K\}$) IoT node is fixed on the ground, denoted by $\mathbf{q}_k = [x_k, y_k]$, where x_k and y_k are the kth IoT node's horizontal plane coordinates. Denote the MEC server's location as $\mathbf{q}_{\mathrm{m}} = [x_{\mathrm{m}}, y_{\mathrm{m}}]$ with the horizontal plane coordinates x_{m} and y_{m}.

Following [22], [23], [24], [25], and [26], the UAV is assumed to fly at a given altitude level, denoted by H ($H > 0$), and its location in the 2-D horizontal plane is given by $\mathbf{q}_u(t) = [x_u(t), y_u(t)]$ with the horizontal plane coordinates $x_u(t)$ and $y_u(t)$ at the time instance t. Assume that both K IoT nodes' locations and the MEC server's location can be obtained at the UAV in order to design the UAV's trajectory [22], [23], [24], [25], [26].

Let T express the duration of the transmission block, which consists of the BackCom phase and the active transmission (AT) phase, respectively. Note that the computing and downloading time at the MEC server can be ignored here due to the fact that the MEC server's computation capacity is sufficiently large, leading to negligible computing and downloading time. Denote β ($0 \le \beta \le 1$) as the time allocation factor. In the BackCom phase with the duration of βT, the UAV keeps flying, and broadcasting energy signals while multiple IoT nodes take turns to perform BackCom. For ease of exposition, the whole BackCom phase is discretized into N equal time slots, and then the duration of the nth ($n \in \mathcal{N} = \{1, 2, \ldots, N\}$) time slot is given by $(\beta T/N)$. Following [22], [23], [24], [25], and [26], we assume that the UAV is static in each time slot. Let $\mathbf{q}_u[n] = [x_u[n], y_u[n]]$ and $g_{n,k}$ denote the location of the UAV and the channel gain from the UAV to the kth IoT node in the nth time slot, respectively. Then, $g_{n,k}$ is given by

$$g_{n,k} = \beta_0 d_{k,n}^{-2} = \frac{\beta_0}{H^2 + \left\|\mathbf{q}_u[n] - \mathbf{q}_k\right\|^2} \tag{1}$$

where β_0 is the channel gain at a reference distance with $d_0 = 1$ m, $d_{k,n}$ denotes the distance from the kth IoT node to the UAV in the nth time slot, and $\|\cdot\|$ expresses the Euclidean norm of a vector. In the AT phase with the duration of $(1-\beta)T$, we consider that multiple IoT nodes take turns to transmit their task bits to avoid the co-channel interference among IoT nodes. Considering that each task can and cannot be partitioned into two parts, two offloading modes, namely, the partial and binary offloading modes, are considered to conduct the task offloading at IoT nodes. The details for the considered network under partial and binary offloading modes are presented below.

A. Partial Offloading Mode

For the partial offloading, each task is partitioned into two parts, where one part will be computed locally and the other will be offloaded to the MEC server for computation. In the following, we will present how the considered network works. Under this mode, the nth time slot in the BackCom phase can be further divided into K subslots, denoted by $t_{n,k}^b$. In the kth subslot of the nth time slot, the kth IoT node modulates its part of computation tasks on a part of its received signals and backscatters the modulated signals for task offloading. The rest part of its received signals is used for EH. Note that the IoT nodes who do not perform BackCom will harvest energy during this period. Let $\alpha_{n,k}$ with $0 \le \alpha_{n,k} \le 1$ denote the power reflection coefficient at the kth IoT node in the nth time slot [27]. Then, the computation bits of the kth IoT node in this time slot is computed by

$$R_{n,k}^b = t_{n,k}^b B \log_2\left(1 + \frac{\xi \alpha_{n,k} P_u g_{n,k} h_k}{B\sigma^2}\right) \tag{2}$$

where B represents the bandwidth of the system, ξ denotes the performance gap[1] reflecting the real modulation, P_u is the UAV's transmit power during the whole transmission block, h_k is the channel power of the kth IoT node-to-the MEC server link, and σ^2 denotes the noise power spectral density. Note that the co-channel interference from the UAV-MEC server link can be canceled by using the successive interference cancelation (SIC). This is because both the energy signals of the UAV and the corresponding channel information are known by the MEC server [28]. Then, at the end of the BackCom phase, the total computation bits of the kth IoT node is given by

$$R_k^b = \sum_{n=1}^{N} R_{n,k}^b = \sum_{n=1}^{N} t_{n,k}^b B \log_2\left(1 + \frac{\xi \alpha_{n,k} P_u g_{n,k} h_k}{B\sigma^2}\right). \tag{3}$$

Correspondingly, the kth IoT node's total harvested energy is given by

$$\begin{aligned} E_{\text{tot}}^k &= \sum_{n=1}^{N} \left[\left(\frac{\beta T}{N} - t_{n,k}^b\right) P_u g_{n,k} \eta + t_{n,k}^b P_u g_{n,k} \eta \left(1 - \alpha_{n,k}\right)\right] \\ &= \sum_{n=1}^{N} \left(\frac{\beta T}{N} P_u g_{n,k} \eta - t_{n,k}^b \alpha_{n,k} P_u g_{n,k} \eta\right) \end{aligned} \tag{4}$$

where η with $0 \le \eta \le 1$ is the energy conversion efficiency. For analytical tractability, we consider a linear EH model, where η is fixed as a constant. Note that this work can be extended to the scenarios with a nonlinear EH model by means of the approach used in [29] or [30].

Likewise, the AT phase is divided into K subslots for K IoT nodes' task offloading. Let p_k and t_k^a express the kth IoT node's transmit power and time, respectively. Then, the computation bits offloaded by the kth IoT node in this phase are given by

$$R_k^a = t_k^a B \log_2\left(1 + \frac{p_k h_k}{B\sigma^2}\right). \tag{5}$$

Based on (3) and (5), we can compute the total achievable computation bits at the kth IoT node as $R_k^{\text{off}} = R_k^b + R_k^a$.

For local computing, let f_k and τ_k ($0 \le \tau_k \le T$) denote local computation frequency and time at the kth IoT node. Then, the kth IoT node's local computation bits are given by

$$R_k^{\text{Loc}} = \frac{f_k \tau_k}{C_{\text{cpu},k}} \tag{6}$$

where $C_{\text{cpu},k}$ reflects the kth IoT node's required number of CPU cycles for computing one bit. Let ε_k be the effective capacitance coefficient of the processor's chip at the kth IoT node. Then, the consumed energy for the kth IoT node's local computation is calculated by

$$E_k^{\text{Loc}} = \varepsilon_k (f_k)^3 \tau_k. \tag{7}$$

[1]Since the backscatter circuit is composed of passive components and is better suited to a simple modulation scheme instead of high-order modulation schemes in practice, there will be a performance gap between the channel capacity of BackCom and the Shannon capacity [18], [28].

B. Binary Offloading Mode

Under this mode, each IoT node either performs complete task offloading or performs fully local computing. Specifically, K IoT nodes can be divided into two sets, which are the set of IoT nodes who perform fully local computing and the set of IoT nodes who perform complete task offloading, respectively. Let $\mathcal{K}_L$ and $\mathcal{K}_O$ denote the above two sets, where $\mathcal{K} = \mathcal{K}_L \cup \mathcal{K}_O$ and $\mathcal{K}_L \cap \mathcal{K}_O = \emptyset$, where $\emptyset$ is the empty set. For the IoT node belonging to $\mathcal{K}_L$, namely, $i \in \mathcal{K}_L$, its total harvested energy is given by

$$E_i^{L,B} = \sum_{n=1}^{N} P_u g_{n,i} \eta \frac{\beta T}{N}, i \in \mathcal{K}_L. \tag{8}$$

Accordingly, its computed bits are given by

$$R_i^{L,B} = \frac{f_i \tau_i}{C_{\text{cpu},i}}, i \in \mathcal{K}_L. \tag{9}$$

For the IoT node belonging to $\mathcal{K}_O$, namely, $l \in \mathcal{K}_O$, its total harvested energy can be expressed as follows:

$$E_l^{O,B} = \sum_{n=1}^{N} \left(\frac{\beta T}{N} P_u g_{n,l} \eta - t_{n,l}^b \alpha_{n,l} P_u g_{n,l} \eta \right), l \in \mathcal{K}_O. \tag{10}$$

Then, its corresponding computed bits are given by

$$R_l^{O,B} = \sum_{n=1}^{N} t_{n,l}^b B \log_2 \left(1 + \frac{\xi \alpha_{n,l} P_u g_{n,l} h_l}{B\sigma^2} \right) + t_l^a B \log_2 \left(1 + \frac{p_l h_l}{B\sigma^2} \right), l \in \mathcal{K}_O. \tag{11}$$

In the following two sections, we will study the WSCB maximization under the partial and binary offloading modes, respectively.

III. Partial Offloading-Based WSCB Maximization

Considering the partial offloading mode at each IoT node, we first formulate a WSCB maximization problem by optimizing the BackCom time, the AT time allocation, the local computing frequencies and time, the reflection coefficients, and the transmit powers of the IoT nodes, as well as the UAV's trajectory, subject to the constraints of the Quality-of-Service (QoS), energy causality, time, speed, the initial and final horizontal location, etc. The formulated problem is highly nonconvex. To solve it, we propose a two-stage alternating algorithm to determine its solution.

A. Problem Formulation

The goal is to maximize the WSCB achieved by all IoT nodes for the considered network. Denote $w_k > 0$ as the weight of the kth IoT node. Then w_k indicates the priority of the kth IoT node in the WSCB maximization problem and can be used to customize the service provisioning for different IoT nodes. Accordingly, the optimization problem is given by

$$\begin{aligned}
\mathbf{P}_1 : \max_{\mathcal{V}} \ & \sum_{k=1}^{K} w_k \left(R_k^{\text{off}} + R_k^{\text{Loc}} \right) \\
\text{s.t.} \ & \text{C1} : R_k^{\text{off}} + R_k^{\text{Loc}} \geq L_{\min,k} \quad \forall k \\
& \text{C2} : E_k^{\text{Loc}} + P_{\text{c},k} \left(\sum_{n=1}^{N} t_{n,k}^b \right) + p_k t_k^a + p_{\text{c},k} t_k^a \\
& \leq E_{\text{tot}}^k \quad \forall k \\
& \text{C3} : 0 \leq f_k \leq f_k^{\max} \quad \forall k \\
& \text{C4} : 0 < \beta < 1, \sum_{k=1}^{K} t_{n,k}^b \leq \frac{\beta T}{N} \quad \forall n \\
& \sum_{k=1}^{K} t_k^a \leq (1-\beta) T \\
& \text{C5} : 0 \leq \tau_k \leq T \quad \forall k \\
& \text{C6} : 0 \leq \alpha_{n,k} \leq 1 \quad \forall k \quad \forall n \\
& \text{C7} : t_{n,k}^b \geq 0 \quad \forall n \quad \forall k, t_k^a \geq 0, p_k \geq 0 \quad \forall k \\
& \text{C8} : \left\| \mathbf{q}_u[n+1] - \mathbf{q}_u[n] \right\| \leq V_{\max} \frac{\beta T}{N} \quad \forall n \\
& \text{C9} : \mathbf{q}_u[1] = \mathbf{q}_{\text{I}}, \mathbf{q}_u[N+1] = \mathbf{q}_F
\end{aligned}$$

where $\mathcal{V} = \{\beta, \{t_{n,k}^b\}, \{t_k^a\}, \{p_k\}, \{f_k\}, \{\tau_k\}, \{\alpha_{n,k}\}, \{\mathbf{q}_u\}\}$ is the set of the optimization variables, $L_{\min,k}$ denotes the minimum required computation bits for the kth IoT node, $P_{\text{c},k}$ and $p_{\text{c},k}$ are the fixed power consumption at the kth IoT node when performing BackCom and AT, respectively, $f_k^{\max}$ expresses the kth IoT node's maximum allowed computation frequency, $V_{\max}$ is the UAV's maximum speed, and $\mathbf{q}_{\text{I}}$ and $\mathbf{q}_F$ denote the initial and final horizontal locations of the UAV. Note that a constant circuit power consumption rate for BackCom is assumed by following [31], [32], and [33] and then the consumed energy for BackCom at the kth IoT node in the nth time slot is computed as $P_{\text{c},k} t_{n,k}^b$.

In the above optimization problem, C1 is the QoS constraint per IoT node. C2 denotes the energy-causality constraint for each IoT node, where each IoT node's total energy consumption for task offloading and execution can not be larger than its harvested energy. C3 limits the maximum computing frequency at each IoT node during the whole transmission block. C4 is the time allocation constraint for BackCom and AT phases while C5 guarantees the local computing time at each IoT node. C6 constrains the value of the power reflection coefficient at each IoT node. C8 represents the speed constraint while C9 is the constraint of the UAV's initial and final horizontal location.

By observing $\mathbf{P_1}$, we find that $\mathbf{P_1}$ is nonconvex due to the existence of several coupled relationships among different variables, i.e., $t_{n,k}^b$, $\alpha_{n,k}$, etc., leading to nonconvex objective function and constraints. Besides, the optimization of the trajectory of the UAV greatly improves the complexity of $\mathbf{P_1}$, bringing a great challenge to solve it.

B. Solution

As for $\mathbf{P_1}$, there is no standard methods to jointly optimize the UAV's trajectory and communication/computation resources. In order to solve $\mathbf{P_1}$, the block coordinate decent (BCD) technique is used to decouple $\mathbf{P_1}$ into two subproblems first, and then a two-stage alternating iterative algorithm is proposed to obtain the solution to $\mathbf{P_1}$. Note that the BCD technique can be used to obtain a locally optimal solution

to a nonconvex problem that cannot be optimally solved by using the existing methods.

Specifically, with a fixed trajectory, the following subproblem can be obtained:

$$\mathbf{P_{1a}}: \max_{\mathcal{V}_1} \sum_{k=1}^{K} w_k\left(R_k^{\text{off}}+R_k^{\text{Loc}}\right) \quad \text{s.t. C1-C7,}$$

where $\mathcal{V}_1=\{\beta,\{t_{n,k}^b\},\{t_k^a\},\{p_k\},\{f_k\},\{\tau_k\},\{\alpha_{n,k}\}\}$.

In order to simplify $\mathbf{P_{1a}}$, Proposition 1 is presented to decide the kth IoT node's optimal computation time, denoted by τ_k^*.

Proposition 1: For achieving the maximum WSCB of all the IoT nodes in the considered network under the partial offloading mode, each IoT node should perform local computation throughout the transmission block, i.e., $\tau_k^*=T$.

Proof: Please see Appendix A. ∎

According to Proposition 1, $\mathbf{P_{1a}}$ can be reformulated as follows:

$$\begin{aligned}\mathbf{P_{2a}}: \max_{\mathcal{V}_2} \ & \sum_{k=1}^{K} w_k\left(R_k^{\text{off}}+\frac{f_kT}{C_{\text{cpu},k}}\right)\\ \text{s.t. } & \text{C1-1}: R_k^{\text{off}}+\frac{f_kT}{C_{\text{cpu},k}}\geq L_{\min,k} \quad \forall k\\ & \text{C2-1}: \varepsilon_k(f_k)^3T+P_{\text{c},k}\left(\sum_{n=1}^{N}t_{n,k}^b\right)+p_kt_k^a+p_{\text{c},k}t_k^a\\ & \leq E_{\text{tot}}^k \quad \forall k\\ & \text{C3, C4, C6, C7}\end{aligned}$$

where $\mathcal{V}_2=\{\beta,\{t_{n,k}^b\},\{t_k^a\},\{p_k\},\{f_k\},\{\alpha_{n,k}\}\}$.

It can be seen that $\mathbf{P_{2a}}$ is still a nonconvex problem and challenge to solve. This is because the coupled relationship between p_k and t_k^a or between $\alpha_{n,k}$ and $t_{n,k}^b$ leads to the nonconvexities of the objective function, C1-1 and C2-1. To address this problem, several auxiliary variables are introduced into $\mathbf{P_{2a}}$. Specifically, let $P_k=p_kt_k^a$ and $x_{n,k}=\alpha_{n,k}t_{n,k}^b \ \ \forall n \ \ \forall k$ replace p_k and $\alpha_{n,k}$, respectively. Then, $\mathbf{P_{2a}}$ can be transformed into

$$\begin{aligned}\mathbf{P_{3a}}: \max_{\mathcal{V}_3} \ & \sum_{k=1}^{K} w_k\left(\sum_{n=1}^{N}t_{n,k}^bB\log_2\left(1+\frac{\xi x_{n,k}P_ug_{n,k}h_k}{t_{n,k}^bB\sigma^2}\right)\right.\\ & \left.+t_k^aB\log_2\left(1+\frac{P_kh_k}{t_k^aB\sigma^2}\right)+\frac{f_kT}{C_{\text{cpu},k}}\right)\\ \text{s.t. } & \text{C1-2}: \sum_{n=1}^{N}t_{n,k}^bB\log_2\left(1+\frac{\xi x_{n,k}P_ug_{n,k}h_k}{t_{n,k}^bB\sigma^2}\right)\\ & +t_k^aB\log_2\left(1+\frac{P_kh_k}{t_k^aB\sigma^2}\right)+\frac{f_kT}{C_{\text{cpu},k}}\geq L_{\min,k} \quad \forall k\\ & \text{C2-2}: \varepsilon_k(f_k)^3T+P_{\text{c},k}\left(\sum_{n=1}^{N}t_{n,k}^b\right)+P_k+p_{\text{c},k}t_k^a\\ & \leq \sum_{n=1}^{N}\left(\frac{\beta T}{N}P_ug_{n,k}\eta-x_{n,k}P_ug_{n,k}\eta\right) \quad \forall k\\ & \text{C3, C4, C6-1}: 0\leq x_{n,k}\leq t_{n,k}^b \quad \forall k \quad \forall n\\ & \text{C7-1}: t_{n,k}^b\geq 0 \quad \forall n \quad \forall k, t_k^a\geq 0, P_k\geq 0 \quad \forall k\end{aligned}$$

where $\mathcal{V}_3=\{\beta,\{t_{n,k}^b\},\{t_k^a\},\{P_k\},\{f_k\},\{x_{n,k}\}\}$.

Proposition 2: $\mathbf{P_{3a}}$ is convex and can be solved by means of several convex tools, i.e., the Lagrange duality method.

Proof: Please see Appendix B. ∎

In Theorem 1, the Lagrange duality method is employed to achieve the optimal solutions to several optimization variables under a given trajectory, as an effort to gain more insights.

Theorem 1: Under a given trajectory $\mathbf{q}_u$, the optimal power reflection coefficient in the nth time slot $\alpha_{n,k}^*$, transmit power p_k^*, and local computing frequency f_k^* of the kth IoT node are determined by

$$\alpha_{n,k}^*=\left[\frac{(w_k+\theta_k)B}{\left(\varpi_kP_ug_{n,k}\eta+\varphi_{n,k}\right)\ln 2}-\frac{B\sigma^2}{\xi P_ug_{n,k}h_k}\right]^+ \quad \forall n \quad \forall k \tag{12}$$

$$p_k^*=\left[\frac{(w_k+\theta_k)B}{\varpi_k\ln 2}-\frac{B\sigma^2}{h_k}\right]^+ \quad \forall k \tag{13}$$

$$f_k^*=\sqrt{\frac{(w_k+\theta_k)}{3\varpi_k\varepsilon_kC_{\text{cpu},k}}-\frac{\phi_k}{3\varpi_k\varepsilon_kT}} \quad \forall k \tag{14}$$

where $\boldsymbol{\theta}=(\theta_1,\theta_2,\ldots,\theta_K)$, $\boldsymbol{\varpi}=(\varpi_0,\varpi_1,\varpi_2,\ldots,\varpi_K)$, $\boldsymbol{\phi}=(\phi_1,\phi_2,\ldots,\phi_K)$, $\boldsymbol{\mu}=(\mu_0,\mu_1,\ldots,\mu_N)$, and

$$\boldsymbol{\varphi}=\begin{pmatrix}\varphi_{1,1} & \cdots & \varphi_{1,K}\\ \vdots & \ddots & \vdots\\ \varphi_{N,1} & \cdots & \varphi_{N,K}\end{pmatrix}$$

are the nonnegative Lagrange multipliers with respect to all the constraints for $\mathbf{P_{3a}}$, namely, C1-2, C2-2, C3, C4, and C6-1.

Proof: Please see Appendix C. ∎

Based on Theorem 1, we have the following findings. First, the maximum WSCB of all IoT nodes is achieved when each IoT node uses up all its harvested energy. Second, the task offloading is chosen by the kth IoT node only when the channel gain from the kth IoT node to the MEC server is strong enough, i.e., $h_k>(\sigma^2\varpi_k\ln 2/w_k+\theta_k)$. Moreover, as for the kth IoT node, when its weight is large, it prefers to perform task offloading. Third, the kth IoT node performs local computation only when $([(w_k+\theta_k)]/[C_{\text{cpu},k}])>(\phi_k/T)$ holds and a larger weight of the kth IoT node brings a larger computation frequency at the kth IoT node. The reasons are as follows. From (12)–(14), it can be observed that $\varpi_k>0$ must hold for achieving the maximum WSCB of all IoT nodes. Then using the Karush–Kuhn–Tucker (KKT) conditions, the equation $\varpi_k(\sum_{n=1}^{N}([\beta T/N]P_ug_{n,k}\eta-x_{n,k}P_ug_{n,k}\eta)-\varepsilon_k(f_k)^3T-P_k-P_{\text{c},k}(\sum_{n=1}^{N}t_{n,k}^b)-p_{\text{c},k}t_k^a)=0$ should always hold. Combining with $\varpi_k>0$, we can obtain $\sum_{n=1}^{N}((\beta T/N)P_ug_{n,k}\eta-x_{n,k}P_ug_{n,k}\eta)-P_{\text{c},k}(\sum_{n=1}^{N}t_{n,k}^b)-\varepsilon_k(f_k)^3T-P_k-p_{\text{c},k}t_k^a=0$, which indicates that the harvested energy per IoT node will be used up. Thus, the first finding is obtained. Based on (13), we can see that $h_k>([\sigma^2\varpi_k\ln 2]/[w_k+\theta_k])$ should be satisfied to guarantee a nonzero p_k^* and the larger the kth IoT node's weight is, the higher the probability with $h_k>(\sigma^2\varpi_k\ln 2/w_k+\theta_k)$ holds, resulting in the fact that the kth IoT node prefers to perform task offloading. Then, the second finding is achieved. Based on (14), in order to obtain a nonzero f_k^*, $([(w_k+\theta_k)]/[C_{\text{cpu},k}])>(\phi_k/T)$ must be satisfied and f_k^* will increase with the increasing of w_k. Therefore, the third finding is obtained.

When the communication resource allocation scheme is given, the trajectory optimization problem is given by

$$\mathbf{P_{1b}}: \max_{\mathbf{q}_u[n]} \sum_{k=1}^{K} w_k \left(\sum_{n=1}^{N} t_{n,k}^b B \log_2 \left(1 + \frac{\xi \alpha_{n,k} P_u h_k \beta_0}{B\sigma^2 \left(H^2 + \left\| \mathbf{q}_u[n] - \mathbf{q}_k \right\|^2 \right)} \right) + R_k^a + R_k^{\mathrm{Loc}} \right)$$

$$\text{s.t.} \quad \mathrm{C1}: \sum_{n=1}^{N} t_{n,k}^b B \log_2 \left(1 + \frac{\xi \alpha_{n,k} P_u h_k \beta_0}{B\sigma^2 \left(H^2 + \left\| \mathbf{q}_u[n] - \mathbf{q}_k \right\|^2 \right)} \right) + R_k^a + R_k^{\mathrm{Loc}} \geq L_{\min,k} \quad \forall k$$

$$\mathrm{C2}: E_k^{\mathrm{Loc}} + P_{\mathrm{c},k} \left(\sum_{n=1}^{N} t_{n,k}^b \right) + p_k t_k^a + p_{\mathrm{c},k} t_k^a \leq \sum_{n=1}^{N} \frac{\beta_0 \left(\frac{\beta T}{N} P_u \eta - t_{n,k}^b \alpha_{n,k} P_u \eta \right)}{H^2 + \left\| \mathbf{q}_u[n] - \mathbf{q}_k \right\|^2} \quad \forall k$$

C8, C9.

Clearly, the objective function, C1 and C2 are nonconvex with respect to $\mathbf{q}_u[n]$, leading to the nonconvex problem $\mathbf{P_{1b}}$. To address it, the successive convex approximation (SCA) method is applied, where its main idea is to successively maximize a lower bound of $\mathbf{P_{1b}}$ via optimizing the incremental of the UAV's trajectory at each iteration. Specifically, let $\mathbf{q}_{u,j}[n] \ \forall n$, denote the local trajectory of the UAV at the jth iteration. Then at the $(j+1)$th iteration, we have the following inequalities, given by:

$$\begin{aligned} R_{k,j+1}^b &= \sum_{n=1}^{N} t_{n,k}^b B \log_2 \left(1 + \frac{\xi \alpha_{n,k} P_u h_k \beta_0}{B\sigma^2 \left(H^2 + \left\| \mathbf{q}_{u,j+1}[n] - \mathbf{q}_k \right\|^2 \right)} \right) \\ &\geq R_{k,j+1}^{b,low} = \sum_{n=1}^{N} t_{n,k}^b B \log_2 \left(1 + \frac{A_{n,k}}{H^2 + \left\| \mathbf{q}_{u,j}[n] - \mathbf{q}_k \right\|^2} \right) \\ &\quad - \sum_{n=1}^{N} \frac{t_{n,k}^b B A_{n,k}}{\left(H^2 + \left\| \mathbf{q}_{u,j}[n] - \mathbf{q}_k \right\|^2 \right) \left(H^2 + \left\| \mathbf{q}_{u,j}[n] - \mathbf{q}_k \right\|^2 + A_{n,k} \right)} \\ &\quad \times \frac{\left(\left\| \mathbf{q}_{u,j+1}[n] - \mathbf{q}_k \right\|^2 - \left\| \mathbf{q}_{u,j}[n] - \mathbf{q}_k \right\|^2 \right)}{\ln 2} \quad \forall k \end{aligned} \tag{15}$$

$$\begin{aligned} E_{\mathrm{tot}}^{k,j+1} &= \sum_{n=1}^{N} \frac{\beta_0 \left(\frac{\beta T}{N} P_u \eta - t_{n,k}^b \alpha_{n,k} P_u \eta \right)}{H^2 + \left\| \mathbf{q}_{u,j+1}[n] - \mathbf{q}_k \right\|^2} \geq E_{\mathrm{tot,low}}^{k,j+1} \\ &= \sum_{n=1}^{N} \frac{B_{n,k}}{H^2 + \left\| \mathbf{q}_{u,j}[n] - \mathbf{q}_k \right\|^2} - \sum_{n=1}^{N} \frac{B_{n,k}}{\left(H^2 + \left\| \mathbf{q}_{u,j}[n] - \mathbf{q}_k \right\|^2 \right)^2} \\ &\quad \times \left(\left\| \mathbf{q}_{u,j+1}[n] - \mathbf{q}_k \right\|^2 - \left\| \mathbf{q}_{u,j}[n] - \mathbf{q}_k \right\|^2 \right) \quad \forall k \end{aligned} \tag{16}$$

where $R_{k,j+1}^b$ and $E_{\mathrm{tot}}^{k,j+1}$ denote the total computation bits and harvested energy at the kth IoT node during the BackCom phase in the $(j+1)$th iteration, $\mathbf{q}_{u,j+1}[n] \ \forall n$, is the UAV's trajectory in the $(j+1)$th iteration, $R_{k,j+1}^{b,low}$ and $E_{\mathrm{tot,low}}^{k,j+1}$ are the low bounds of $R_{k,j+1}^b$ and $E_{\mathrm{tot}}^{k,j+1}$, respectively, $A_{n,k} = ([\xi \alpha_{n,k} P_u h_k \beta_0]/[B\sigma^2])$, and $B_{n,k} = \beta_0([\beta T/N] P_u \eta - t_{n,k}^b \alpha_{n,k} P_u \eta)$.

Based on (15) and (16), we optimize the trajectory of the UAV in the $(j+1)$th iteration by replacing $R_{k,j+1}^b$ and $E_{\mathrm{tot}}^{k,j+1}$ with their low bounds, namely, $R_{k,j+1}^{b,low}$ and $E_{\mathrm{tot,low}}^{k,j+1}$. Accordingly, $\mathbf{P_{1b}}$ of the $(j+1)$th iteration is transformed into

$$\mathbf{P_{2b}}: \max_{\mathbf{q}_{u,j+1}[n]} \sum_{k=1}^{K} w_k \left(R_{k,j+1}^{\mathrm{b,low}} + R_k^a + R_k^{\mathrm{Loc}} \right)$$

$$\text{s.t.} \quad \mathrm{C1\text{-}3}: R_{k,j+1}^{\mathrm{b,low}} + R_k^a + R_k^{\mathrm{Loc}} \geq L_{\min,k} \quad \forall k$$

$$\mathrm{C2\text{-}3}: E_k^{\mathrm{Loc}} + P_{\mathrm{c},k} \left(\sum_{n=1}^{N} t_{n,k}^b \right) + p_k t_k^a + p_{\mathrm{c},k} t_k^a \leq E_{\mathrm{tot,low}}^{k,j+1} \quad \forall k$$

$$\mathrm{C8\text{-}1}: \left\| \mathbf{q}_{u,j+1}[n+1] - \mathbf{q}_{u,j+1}[n] \right\| \leq V_{\max} \frac{\beta T}{N} \quad \forall n$$

$$\mathrm{C9\text{-}1}: \ \mathbf{q}_{u,j+1}[1] = \mathbf{q}_{\mathrm{I}}, \mathbf{q}_{u,j+1}[N+1] = \mathbf{q}_F.$$

Since both $R_{k,j+1}^{b,low}$ and $E_{\mathrm{tot,low}}^{k,j+1}$ are concave functions regarding to $\mathbf{q}_{u,j+1}[n]$, $\mathbf{P_{2b}}$ is convex and can be solved by means of several convex tools, i.e., the interior point method. On this basis, we propose a successive trajectory optimization algorithm, as shown in Algorithm 1, to achieve the UAV's trajectory with fixed communication resource allocation. Specifically, $\mathbf{P_{2b}}$ should be optimally solved by means of the convex tools, i.e., CVX [34], in each iteration and the above step continues until the stopping condition is satisfied.

Algorithm 1 Successive Trajectory Optimization With Fixed Communication Resource Allocation

1: Initialize the UAV's trajectory as $\mathbf{q}_{\mathrm{u},0}[n] \ \forall n$, and set $j = 0$;
2: Set the maximum allowed number of iterations as $I_{\max}$ and Flag $= 0$;
3: **repeat**
4: Solve $\mathbf{P_{2b}}$ and obtain the optimal trajectory as $\mathbf{q}_{\mathrm{u},j+1}[n] \ \forall n$;
5: **if** $\mathbf{q}_{\mathrm{u},j+1}[n]$ is converge to $\mathbf{q}_{\mathrm{u},j}[n] \ \forall n$ **then**
6: Set $\mathbf{q}_{\mathrm{u}}^*[n] = \mathbf{q}_{\mathrm{u},j+1}[n], \forall n$ and set Flag $= 1$;
7: **else**
8: Set $j = j + 1$ and Flag $= 0$;
9: **end if**
10: **until** $j = I_{\max}$ or Flag $= 1$.

C. Design of Two-Stage Alternating Iterative Algorithm

Here, we propose a two-stage alternating iterative algorithm to solve $\mathbf{P_1}$ and the detailed process is shown in Algorithm 2. Specifically, we take turns to solve $\mathbf{P_{3a}}$ and $\mathbf{P_{1b}}$ and obtain their optimal solutions in each iteration. Note that $\mathbf{P_{3a}}$ is optimally solved by means of CVX, while $\mathbf{P_{1b}}$ is solved by using Algorithm 1. The above steps will continue until the stopping condition is satisfied.

The complexity of the proposed two-stage alternating iterative algorithm in Algorithm 2 is provided as follows. Assume that the interior point method is applied to obtain the optimal solutions to $\mathbf{P_{3a}}$ and $\mathbf{P_{2b}}$. According to [34], the complexities for solving $\mathbf{P_{3a}}$ and $\mathbf{P_{2b}}$ are computed as $O(\sqrt{5K + 2KN + 3} \log(5K + 2KN + 3))$ and $O(\sqrt{2K + N} \log(2K + N))$, where $O(\cdot)$ is the big-O notation. Let N_1 and N_2 denote the number of iterations of Algorithms 1 and 2, then the complexity of the proposed two-stage alternating iterative algorithm is given by $N_2(O(\sqrt{5K + 2KN + 3} \log(5K + 2KN + 3)) + N_1 O(\sqrt{2K + N} \log(2K + N)))$.

Algorithm 2 Two-Stage Alternating Iterative Algorithm

1: Initialize the trajectory of the UAV and the maximum tolerance error δ_t;
2: **repeat**
3: Solve $\mathbf{P}_{3a}$ with the fixed UAV's trajectory via CVX and obtain the optimal communication resource allocation;
4: Compute the WSCB of all IoT nodes as R^1_{sum};
5: Solve $\mathbf{P}_{1b}$ with the fixed communication resource allocation obtained in the above step by using Algorithm 1 and obtain the UAV's trajectory;
6: Compute the WSCB of all IoT nodes as R^2_{sum};
7: **until** $|R^2_{\text{sum}} - R^1_{\text{sum}}| \le \delta_t$;
8: Output the obtained communication resource allocation and trajectory.

IV. Binary Offloading-Based WSCB Maximization

In this section, considering the binary offloading mode at each IoT node, the WSCB maximization is studied for the UAV-enabled WP-MEC network with hybrid passive and ACs. Specifically, by formulating the WSCB maximization problem for the considered network, the local computation frequencies and time, the reflection coefficients, the transmit powers, the BackCom time and the AT time of IoT nodes, the trajectory of the UAV, as well as the mode selection of each IoT node for choosing either task offloading or local computation are jointly optimized. The formulated problem not only involves the optimization of the UAV's trajectory, but also includes the optimization of the mode selection, leading to a mixed-integer nonconvex optimization problem. To address this problem, a three-stage alternating iterative algorithm is devised.

A. Problem Formulation

Based on (9) and (11), the WSCB maximization problem under the binary offloading mode is formulated as follows:

$$\mathbf{P}_4: \max_{\mathcal{V}_4} \sum_{i\in\mathcal{K}_L} w_i R_i^{\text{L,B}} + \sum_{l\in\mathcal{K}_O} w_l R_l^{\text{O,B}}$$
$$\text{s.t.} \quad \text{F1}: R_i^{\text{L,B}} \ge L_{\min,i}, i\in\mathcal{K}_L, R_l^{\text{O,B}} \ge L_{\min,l}, l\in\mathcal{K}_O$$
$$\text{F2}: E_i^{\text{Loc}} \le E_i^{\text{L,B}}, i\in\mathcal{K}_L, P_{\text{c},l}\left(\sum_{n=1}^{N} t_{n,l}^b\right) + p_l t_l^a + p_{\text{c},l} t_l^a \le E_l^{\text{O,B}}, l\in\mathcal{K}_O$$
$$\text{F3}: 0 \le f_i \le f_i^{\max}, i\in\mathcal{K}_L$$
$$\text{F4}: 0<\beta<1, \sum_{l\in\mathcal{K}_O} t_{n,l}^b \le \frac{\beta T}{N} \quad \forall n, \sum_{l\in\mathcal{K}_O} t_l^a \le (1-\beta)T$$
$$\text{F5}: 0 \le \tau_i \le T, i\in\mathcal{K}_L$$
$$\text{F6}: 0 \le \alpha_{n,l} \le 1, l\in\mathcal{K}_O \quad \forall n$$
$$\text{F7}: t_{n,l}^b \ge 0 \quad \forall n, t_l^a \ge 0, p_l \ge 0, l\in\mathcal{K}_O$$
$$\text{F8}: \mathcal{K}_L \cup \mathcal{K}_O = \mathcal{K}, \mathcal{K}_L \cap \mathcal{K}_O = \emptyset$$
$$\text{F9}: \left\|\mathbf{q}_u[n+1] - \mathbf{q}_u[n]\right\| \le V_{\max}\frac{\beta T}{N} \quad \forall n$$
$$\text{F10}: \mathbf{q}_u[1] = \mathbf{q}_{\text{I}}, \mathbf{q}_u[N+1] = \mathbf{q}_F$$

where $\mathcal{V}_4 = \{\beta, \{t_{n,l}^b\}, \{t_l^a\}, \{p_l\}, \{f_i\}, \{\tau_i\}, \{\alpha_{n,l}\}, \mathcal{K}_L, \mathcal{K}_O, \{\mathbf{q}_u\}\}$.

In $\mathbf{P}_4$, F1 and F2 are the minimum tasks requirement and the energy causal constraints per IoT node, respectively. F3 constrains the maximum allowed computation frequency at the IoT node who performs fully local computation. Both F4 and F5 are time allocation constrains which ensure that the total consumed time for task execution is not larger than T. F6 indicates the range of the power reflection coefficient of the IoT node who chooses to offload tasks. F8 is the user operation selection constraint, where each IoT node either computes its tasks locally or performs task offloading. F9 is the speed constraint and F10 constrains the UAV's initial and final horizontal location.

$\mathbf{P}_4$ is a mixed-integer nonconvex problem due to the following reasons. First, $\mathbf{P}_4$ involves the optimization of the user mode selection. Second, the optimization of the trajectory of the UAV exists in $\mathbf{P}_4$, bringing coupled relationships between the trajectory and communication/computation resources. Third, the coupled relationships among different optimization variables of communication/computation resources further increase the difficulty of solving $\mathbf{P}_4$.

B. Solution

Similar to $\mathbf{P}_1$, here $\mathbf{P}_4$ is decoupled into two subproblems, where one subproblem is $\mathbf{P}_4$ with a fixed trajectory, denoted by $\mathbf{P}_{4a}$, and the other is $\mathbf{P}_4$ with fixed communication resources, namely, $\mathbf{P}_{4b}$, respectively. Accordingly, $\mathbf{P}_{4a}$ can be formulated as follows:

$$\mathbf{P}_{4a}: \max_{\mathcal{V}_5} \sum_{i\in\mathcal{K}_L} w_i R_i^{\text{L,B}} + \sum_{l\in\mathcal{K}_O} w_l R_l^{\text{O,B}}$$
$$\text{s.t.} \quad \text{F1-F8}$$

where $\mathcal{V}_5 = \{\beta, \{t_{n,l}^b\}, \{t_l^a\}, \{p_l\}, \{f_i\}, \{\tau_i\}, \{\alpha_{n,l}\}, \mathcal{K}_L, \mathcal{K}_O\}$.

It is obvious that $\mathbf{P}_{4a}$ is still a nonconvex problem. To address this problem, we first introduce the following proposition to clarify the optimal computing time of the IoT node that performs local computation and decouples the coupled relationship between the computing frequency and time of the IoT node.

Proposition 3: The WSCB of all the IoT nodes for the considered network under the binary offloading mode are maximized when the IoT node that performs local computation executes its tasks during the whole transmission block, i.e., $\tau_i = T, i\in\mathcal{K}_L$.

Proof: This proposition can be proved by means of contradictions and the process of the proof is similar to Appendix A. Therefore, the detailed process is omitted. ■

According to Proposition 3, $\mathbf{P}_{4a}$ can be transformed as follows:

$$\mathbf{P}_{5a}: \max_{\mathcal{V}_6} \sum_{i\in\mathcal{K}_L} \frac{w_i f_i T}{C_{\text{cpu},i}} + \sum_{l\in\mathcal{K}_O} w_l R_l^{\text{O,B}}$$
$$\text{s.t.} \quad \text{F1-1}: \frac{f_i T}{C_{\text{cpu},i}} \ge L_{\min,i}, i\in\mathcal{K}_L, R_l^{\text{O,B}} \ge L_{\min,l}, l\in\mathcal{K}_O$$
$$\text{F2-1}: \varepsilon_i (f_i)^3 T \le E_i^{\text{L,B}}, i\in\mathcal{K}_L$$

$$P_{\mathrm{c},l}\left(\sum_{n=1}^{N} t_{n,l}^{b}\right) + p_l t_l^a + p_{\mathrm{c},l} t_l^a \le E_l^{\mathrm{O,B}}, l \in \mathcal{K}_O$$
$$\text{F3, F4, F6-F8}$$

where $\mathcal{V}_6 = \{\beta, \{t_{n,l}^b\}, \{t_l^a\}, \{p_l\}, \{f_l\}, \{\alpha_{n,l}\}, \mathcal{K}_L, \mathcal{K}_O\}$.

In order to efficiently deal with the optimization of the user mode selection, we introduce a binary variable, denoted by λ_k ($\lambda_k \in \{0, 1\}\ \forall k$), into $\mathbf{P}_{5\mathrm{a}}$, where $\lambda_k = 1$ indicates that the kth IoT node performs task offloading and $\lambda_k = 0$ means that the kth IoT node chooses to compute its tasks locally. Substituting λ_k into $\mathbf{P}_{5\mathrm{a}}$, we have

$$\begin{aligned}
\mathbf{P}_{6\mathrm{a}}: \max_{\mathcal{V}_7}\ & \sum_{k=1}^{K} w_k \left(\lambda_k \left(\sum_{n=1}^{N} t_{n,k}^b B \log_2\left(1+\frac{\xi \alpha_{n,k} P_u g_{n,k} h_k}{B\sigma^2}\right) + t_k^a B \log_2\left(1+\frac{p_k h_k}{B\sigma^2}\right)\right) + (1-\lambda_k)\frac{f_k T}{C_{\mathrm{cpu},k}}\right) \\
\text{s.t.}\ & \text{F1-2}: \lambda_k \left(\sum_{n=1}^{N} t_{n,k}^b B \log_2\left(1+\frac{\xi \alpha_{n,k} P_u g_{n,k} h_k}{B\sigma^2}\right) + t_k^a B \log_2\left(1+\frac{p_k h_k}{B\sigma^2}\right)\right) + \frac{(1-\lambda_k) f_k T}{C_{\mathrm{cpu},k}} \ge L_{\min,k} \quad \forall k \\
& \text{F2-2}: (1-\lambda_k)\varepsilon_k (f_k)^3 T + \lambda_k \left(P_{\mathrm{c},k}\left(\sum_{n=1}^{N} t_{n,k}^b\right) + p_k t_k^a + p_{\mathrm{c},k} t_k^a\right) \le \sum_{n=1}^{N}\left(\frac{\beta T}{N} P_u g_{n,k}\eta - \lambda_k t_{n,k}^b \alpha_{n,k} P_u g_{n,k}\eta\right) \quad \forall k \\
& \text{F3-1}: 0 \le (1-\lambda_k) f_k \le f_k^{\max} \quad \forall k \\
& \text{F4-1}: 0 < \beta < 1, \sum_{k=1}^{K} \lambda_k t_{n,k}^b \le \frac{\beta T}{N} \quad \forall n \\
& \sum_{k=1}^{K} \lambda_k t_k^a \le (1-\beta) T \\
& \text{F6-1}: 0 \le \lambda_k \alpha_{n,k} \le 1 \quad \forall k \quad \forall n \\
& \text{F7-1}: t_{n,k}^b \ge 0 \quad \forall n, t_k^a \ge 0, p_k \ge 0 \quad \forall k \\
& \text{F8-1}: \lambda_k \in \{0,1\} \quad \forall k
\end{aligned}$$

where $\mathcal{V}_7 = \{\beta, \{t_{n,k}^b\}, \{t_k^a\}, \{p_k\}, \{f_k\}, \{\alpha_{n,k}\}, \lambda_k\}$.

$\mathbf{P}_{6\mathrm{a}}$ is a mixed-integer nonconvex problem. To address the issue arisen from the integer optimization, we relax the integer variable λ_k as a continuous real variable that varies from 0 to 1 by following [35]. Note that such a relaxation removes the integer optimization, bringing a more tractable problem. Thus, $\mathbf{P}_{6\mathrm{a}}$ can be relaxed as follows:

$$\begin{aligned}
\mathbf{P}_{7\mathrm{a}}: \max_{\mathcal{V}_7}\ & \sum_{k=1}^{K} w_k \left(\lambda_k \left(\sum_{n=1}^{N} t_{n,k}^b B \log_2\left(1+\frac{\xi \alpha_{n,k} P_u g_{n,k} h_k}{B\sigma^2}\right) + t_k^a B \log_2\left(1+\frac{p_k h_k}{B\sigma^2}\right)\right) + (1-\lambda_k)\frac{f_k T}{C_{\mathrm{cpu},k}}\right) \\
\text{s.t.}\ & \text{F1-2, F2-2, F3-1, F4-1, F6-1, F7-1} \\
& F8-2: \lambda_k \in [0,1] \quad \forall k.
\end{aligned}$$

However, $\mathbf{P}_{7\mathrm{a}}$ is still nonconvex since the optimization of λ_k is highly coupled with the optimization of other communication resources. To tackle this issue, we also apply the BCD technique to handle $\mathbf{P}_{7\mathrm{a}}$. Specifically, $\mathbf{P}_{7\mathrm{a}}$ can be decoupled into two subproblems: $\mathbf{P}_{7\mathrm{a}}$ with fixed λ_k and $\mathbf{P}_{7\mathrm{a}}$ with other communication resources fixed. When λ_k is fixed, $\mathbf{P}_{7\mathrm{a}}$ is reduced to

$$\begin{aligned}
\mathbf{P}_{8\mathrm{a}}: \max_{\mathcal{V}_8}\ & \sum_{k=1}^{K} w_k \left(\lambda_k \left(\sum_{n=1}^{N} t_{n,k}^b B \log_2\left(1+\frac{\xi \alpha_{n,k} P_u g_{n,k} h_k}{B\sigma^2}\right) + t_k^a B \log_2\left(1+\frac{p_k h_k}{B\sigma^2}\right)\right) + (1-\lambda_k)\frac{f_k T}{C_{\mathrm{cpu},k}}\right) \\
\text{s.t.}\ & \text{F1-2, F2-2, F3-1, F4-1, F6-1, F7-1}
\end{aligned}$$

where $\mathcal{V}_8 = \{\beta, \{t_{n,k}^b\}, \{t_k^a\}, \{p_k\}, \{f_k\}, \{\alpha_{n,k}\}\}$. To deal with the coupled relationships among different optimization variables in $\mathbf{P}_{8\mathrm{a}}$, the following variables are introduced: $x_{n,k} = t_{n,k}^b \alpha_{n,k} \quad \forall n\ \forall k$, and $P_k = p_k t_k^a \quad \forall k$, and then $\mathbf{P}_{8\mathrm{a}}$ can be rewritten as follows:

$$\begin{aligned}
\mathbf{P}_{9\mathrm{a}}: \max_{\mathcal{V}_9}\ & \sum_{k=1}^{K} w_k \left(\lambda_k \left(\sum_{n=1}^{N} t_{n,k}^b B \log_2\left(1+\frac{\xi x_{n,k} P_u g_{n,k} h_k}{t_{n,k}^b B\sigma^2}\right) + t_k^a B \log_2\left(1+\frac{P_k h_k}{t_k^a B\sigma^2}\right)\right) + (1-\lambda_k)\frac{f_k T}{C_{\mathrm{cpu},k}}\right) \\
\text{s.t.}\ & \text{F1-3}: \lambda_k \left(\sum_{n=1}^{N} t_{n,k}^b B \log_2\left(1+\frac{\xi x_{n,k} P_u g_{n,k} h_k}{t_{n,k}^b B\sigma^2}\right) + t_k^a B \log_2\left(1+\frac{P_k h_k}{t_k^a B\sigma^2}\right)\right) + \frac{(1-\lambda_k) f_k T}{C_{\mathrm{cpu},k}} \ge L_{\min,k} \quad \forall k \\
& \text{F2-3}: \lambda_k \left(P_{\mathrm{c},k}\left(\sum_{n=1}^{N} t_{n,k}^b\right) + P_k + p_{\mathrm{c},k} t_k^a\right) + (1-\lambda_k)\varepsilon_k (f_k)^3 T \le \sum_{n=1}^{N}\left(\frac{\beta T}{N} P_u g_{n,k}\eta - \lambda_k x_{n,k} P_u g_{n,k}\eta\right) \quad \forall k \\
& \text{F3-1, F4-1, F6-2}: 0 \le \lambda_k x_{n,k} \le t_{n,k}^b \quad \forall k\ \forall n \\
& \text{F7-2}: t_{n,k}^b \ge 0 \quad \forall n, t_k^a \ge 0, P_k \ge 0 \quad \forall k
\end{aligned}$$

where $\mathcal{V}_9 = \{\beta, \{t_{n,k}^b\}, \{t_k^a\}, \{P_k\}, \{f_k\}, \{x_{n,k}\}\}$. It is easy to prove that $\mathbf{P}_{9\mathrm{a}}$ is convex and the detailed process of the proof is similar to Appendix B and is omitted here for brevity.

When other communication resources are fixed, $\mathbf{P}_{7\mathrm{a}}$ can be transformed as follows:

$$\begin{aligned}
\mathbf{P}_{10\mathrm{a}}: \max_{\{\lambda_k\}}\ & \sum_{k=1}^{K} w_k \left(\lambda_k \left(\sum_{n=1}^{N} t_{n,k}^b B \log_2\left(1+\frac{\xi \alpha_{n,k} P_u g_{n,k} h_k}{B\sigma^2}\right) + t_k^a B \log_2\left(1+\frac{p_k h_k}{B\sigma^2}\right)\right) + (1-\lambda_k)\frac{f_k T}{C_{\mathrm{cpu},k}}\right) \\
\text{s.t.}\ & \text{F1-2, F2-2, F3-1, F4-1, F6-1, F8-2.}
\end{aligned}$$

Obviously, $\mathbf{P}_{10\mathrm{a}}$ is a linear optimization problem regarding to λ_k, which can be solved by means of several convex tools.

Likewise, $\mathbf{P}_{4\mathrm{b}}$ is reformulated as follows:

$$\mathbf{P}_{4\mathrm{b}}: \max_{\mathbf{q}_u[n]} \sum_{k=1}^{K} w_k \left(\lambda_k \left(\sum_{n=1}^{N} t_{n,k}^b B \log_2\left(1+\frac{\xi \alpha_{n,k} P_u h_k \beta_0}{B\sigma^2\left(H^2 + \left\|\mathbf{q}_u[n] - \mathbf{q}_k\right\|^2\right)}\right) + t_k^a B \log_2\left(1+\frac{p_k h_k}{B\sigma^2}\right)\right) + (1-\lambda_k)\frac{f_k T}{C_{\mathrm{cpu},k}}\right)$$

$$
\begin{aligned}
\text{s.t.}\quad & \text{F1-2}: \lambda_k\left(\sum_{n=1}^{N} t_{n,k}^{b} B\log_2\left(1+\frac{\xi\alpha_{n,k}P_u h_k\beta_0}{B\sigma^2\left(H^2+\left\|\mathbf{q}_u[n]-\mathbf{q}_k\right\|^2\right)}\right)\right.\\
& \left.+\, t_k^a B\log_2\left(1+\frac{p_k h_k}{B\sigma^2}\right)\right)+\frac{(1-\lambda_k)f_k T}{C_{\text{cpu},k}}\\
& \geq L_{\min,k} \quad \forall k\\
& \text{F2-2}: \lambda_k\left(P_{\text{c},k}\left(\sum_{n=1}^{N} t_{n,k}^{b}\right)+p_k t_k^a+p_{\text{c},k}t_k^a\right)\\
& +(1-\lambda_k)\varepsilon_k(f_k)^3 T\\
& \leq \sum_{n=1}^{N}\frac{\left(\frac{\beta T}{N}P_u-\lambda_k t_{n,k}^{b}\alpha_{n,k}P_u\right)\beta_0\eta}{\left(H^2+\left\|\mathbf{q}_u[n]-\mathbf{q}_k\right\|^2\right)} \quad \forall k\\
& \text{F9, F10.}
\end{aligned}
$$

In order to solve $\mathbf{P}_{4\text{b}}$, the SCA technique is applied by following $\mathbf{P}_{1\text{b}}$. Accordingly, $\mathbf{P}_{4\text{b}}$ in the $(j+1)$th iteration is transformed into

$$
\begin{aligned}
\mathbf{P}_{5\text{b}}: \max_{\mathbf{q}_u[n]}\ & \sum_{k=1}^{K} w_k\left(\lambda_k\left(R_{k,j+1}^{b}+t_k^a B\log_2\left(1+\frac{p_k h_k}{B\sigma^2}\right)\right)\right.\\
& \left.+(1-\lambda_k)\frac{f_k T}{C_{\text{cpu},k}}\right)\\
\text{s.t.}\quad & \text{F1-4}: \lambda_k\left(R_{k,j+1}^{b}+t_k^a B\log_2\left(1+\frac{p_k h_k}{B\sigma^2}\right)\right)\\
& +\frac{(1-\lambda_k)f_k T}{C_{\text{cpu},k}}\geq L_{\min,k} \quad \forall k\\
& \text{F2-4}: (1-\lambda_k)\varepsilon_k(f_k)^3 T\\
& +\lambda_k\left(P_{\text{c},k}\left(\sum_{n=1}^{N} t_{n,k}^{b}\right)+p_k t_k^a+p_{\text{c},k}t_k^a\right)\\
& \leq E_{\text{tot}}^{k,j+1} \quad \forall k\\
& \text{F9-1}: \left\|\mathbf{q}_{u,j+1}[n+1]-\mathbf{q}_{u,j+1}[n]\right\|\leq V_{\max}\frac{\beta T}{N} \quad \forall n\\
& \text{F10-1}: \mathbf{q}_{u,j+1}[1]=\mathbf{q}_{\text{I}},\ \mathbf{q}_{u,j+1}[N+1]=\mathbf{q}_F
\end{aligned}
$$

where $B_{n,k} = \beta_0([\beta T/N]P_u\eta-\lambda_k t_{n,k}^{b}\alpha_{n,k}P_u\eta)$ in $E_{\text{tot}}^{k,j+1}$. Similar to $\mathbf{P}_{2\text{b}}$, $\mathbf{P}_{5\text{b}}$ is also convex, which can be solved by applying convex tools, e.g., CVX.

C. Design of Three-Stage Alternating Iterative Algorithm

Here, a three-stage alternating iterative algorithm is proposed to solve $\mathbf{P}_4$ and obtain the corresponding resource allocation and trajectory. The steps of this algorithm can be found in Algorithm 3. Specifically, in the outer loop, $\mathbf{P}_{7\text{a}}$ and $\mathbf{P}_{4\text{b}}$ should be solved in each iteration, where $\mathbf{P}_{7\text{a}}$ is solved with fixed trajectory of the UAV and $\mathbf{P}_{4\text{b}}$ is solved under given communication resource allocation. The first inner loop is to solve $\mathbf{P}_{7\text{a}}$, where in each iteration, we take turns to optimally solve $\mathbf{P}_{9\text{a}}$ and $\mathbf{P}_{10\text{a}}$. The second inner loop is to solve $\mathbf{P}_{4\text{b}}$, where $\mathbf{P}_{5\text{b}}$ is optimally solved in each iteration.

As for the proposed three-stage alternating iterative algorithm in Algorithm 3, its complexity is computed as follows. With the interior point method adopted, the complexities for solving $\mathbf{P}_{9\text{a}}$, $\mathbf{P}_{10\text{a}}$, and $\mathbf{P}_{5\text{b}}$ are given by $O(\sqrt{5K+2KN+3}\log(5K+2KN+3))$, $O(\sqrt{4K+KN+3}\log(4K+KN+3))$ and $O(\sqrt{2K+N}\log(2K+N))$, respectively, [34]. Denote L_1, L_2, and L_3 as the number of iterations required for the outer loop, the first inner loop, and the second loop. Then, the computation complexity of the three-stage alternating iterative algorithm can be calculated as $L_1(L_2(O(\sqrt{5K+2KN+3}\log(5K+2KN+3))+O(\sqrt{4K+KN+3}\log(4K+KN+3)))+L_3O(\sqrt{2K+N}\log(2K+N)))$.

Algorithm 3 Three-Stage Alternating Iterative Algorithm

1: Initialize the iterative number $J=1$;
2: Initialize the trajectory of the UAV $\mathbf{q}_{\text{u}}^{J}[n]\ \ \forall n$, and the maximum tolerance errors δ_1 and δ_2;
3: **repeat**
4: Initialize the iterative number $jj=1$ and $\lambda_k^{jj}\ \ \forall k$;
5: **repeat**
6: Solve $\mathbf{P}_{9\text{a}}$ with given $\mathbf{q}_{\text{u}}^{J}[n]\ \ \forall n$, and $\lambda_k^{jj}\ \ \forall k$ via CVX and obtain the optimal communication resource allocation, denoted by $\{\beta^{jj}, \{t_{n,k}^{\text{b},jj}\}, \{t_k^{\text{a},jj}\}, \{P_k^{jj}\}, \{f_k^{jj}\}, \{x_{n,k}^{jj}\}\}$;
7: Compute the WSCB of all IoT nodes as R_{sum}^{jj};
8: Solve $\mathbf{P}_{10\text{a}}$ with given $\{\beta^{jj}, \{t_{n,k}^{\text{b},jj}\}, \{t_k^{\text{a},jj}\}, \{P_k^{jj}\}, \{f_k^{jj}\}, \{x_{n,k}^{jj}\}\}$ and $\mathbf{q}_{\text{u}}^{J}[n]\ \ \forall n$, and obtain $\lambda_k^{jj+1}\ \ \forall k$;
9: Compute the WSCB of all IoT nodes as R_{sum}^{jj+1};
10: **until** $|R_{\text{sum}}^{jj+1}-R_{\text{sum}}^{jj}|\leq\delta_1$;
11: Output the obtained communication resource allocation under $\mathbf{q}_{\text{u}}^{J}[n], \forall n$, and the WSCB of all IoT nodes R_J^s;
12: Initialize the iterative number $j=1$ and the maximum allowed number of iterations $I_{\max}$;
13: Set $\mathbf{q}_{\text{u},j}[n]=\mathbf{q}_{\text{u}}^{J}[n]\ \ \forall n$;
14: **repeat**
15: Solve $\mathbf{P}_{5\text{b}}$ with given $\{\beta^{jj}, \{t_{n,k}^{\text{b},jj}\}, \{t_k^{\text{a},jj}\}, \{P_k^{jj}\}, \{f_k^{jj}\}, \{x_{n,k}^{jj}\}, \{\lambda_k^{jj+1}\}\}$ and obtain the optimal trajectory as $\mathbf{q}_{\text{u},j+1}[n]\ \ \forall n$;
16: **if** $\mathbf{q}_{\text{u},j+1}[n]$ is converge to $\mathbf{q}_{\text{u},j}[n]\ \ \forall n$ **then**
17: Set $J=J+1$, $\mathbf{q}_{\text{u}}^{J}[n]=\mathbf{q}_{\text{u},j+1}[n]\ \ \forall n$ and break;
18: **else**
19: Set $j=j+1$;
20: **end if**
21: **until** $j=I_{\max}$;
22: Output the obtained trajectory and the WSCB achieved by all IoT nodes R_J^s;
23: **until** $|R_J^s-R_{J-1}^s|\leq\delta_2$;
24: Output the obtained resource allocation and trajectory.

V. Simulations

This section validates the superiority of the proposed schemes by conducting computer simulations. The basic settings of the parameters, unless otherwise specified, are shown in Table I according to [4], [10], [15], and [28]. Here, the channel gain of the kth IoT node-the MEC server link is considered as $h_k=h_k'd_k^{-\alpha}$ with the small-scale fading h_k', distance d_k, and path loss exponent α. We set $\alpha=3$, $d_1=12$ m, $d_2=10$ m, $d_3=15$ m, and $d_4=13$ m. The locations of IoT nodes are set as $\mathbf{q}_1=[0,0]$, $\mathbf{q}_2=[0,10]$, $\mathbf{q}_3=[10,10]$, and $\mathbf{q}_4=[10,0]$, respectively. The UAV's initial and final positions are given by $\mathbf{q}_{\text{I}}=[0,0]$ and $\mathbf{q}_F=[10,0]$. The weight vector of all IoT nodes, $[w_1,w_2,w_3,w_4]$, is set as $[0.1,0.4,0.3,0.2]$.

In order to show the advantages of the proposed schemes in terms of the WSCB of all IoT nodes, the performance under the proposed schemes is compared with that under

TABLE I
KEY SIMULATION SETTINGS

Parameters	Notation	Value
Number of IoT nodes	K	4
Number of time slots	N	50
Altitude of the UAV	H	10 m
The maximum speed of the UAV	$V_{\max}$	20 m/s
The entire transmission block	T	2 seconds
The system bandwidth	B	100 kHz
The number of CPU cycles for computing 1 bit at the k-th IoT node	$C_{\mathrm{cpu},k}$	1000 cycles/bit
The BackCom's fixed circuit power consumption at the k-th IoT node	$P_{\mathrm{c},k}$	100 μW
The AT's fixed circuit power consumption at the k-th IoT node	$p_{\mathrm{c},k}$	1 mW
The UAV's transmit power	P_{u}	1 W
The fixed energy conversion efficiency per IoT node	η	0.7
The performance gap reflecting the real modulation for BackCom	ξ	-15 dB
The noise power spectral density	σ^2	-120 dBm/Hz
Channel gain at reference distance	β_0	-30 dB
The effective capacitance coefficient at the k-th IoT node	ε_k	10^{-26}
The maximum CPU frequency of the k-th IoT node	$f_k^{\max}$	500 MHz
The minimum required bits computed by the k-th IoT node	$L_{\min,k}$	10 kbits

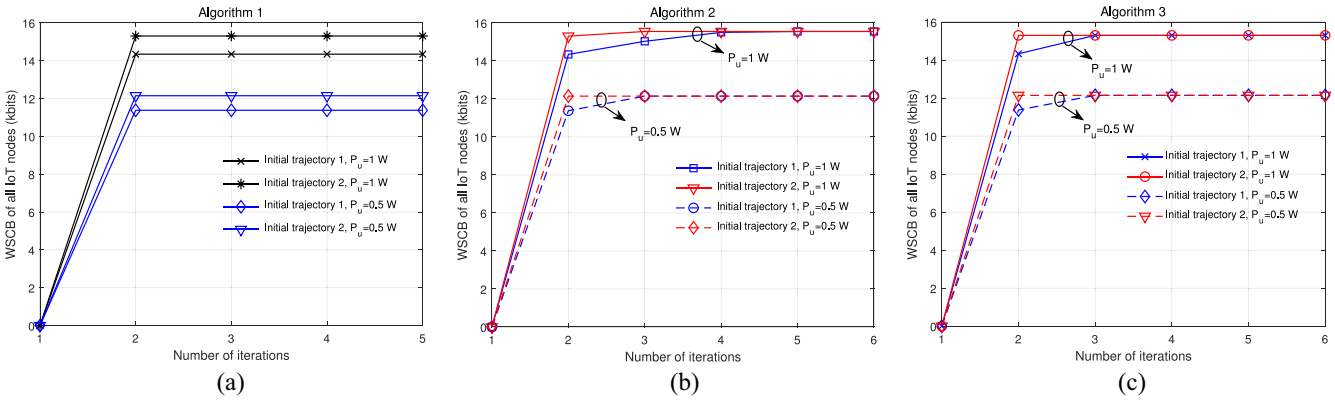

Fig. 2. Convergence analysis of the proposed iterative algorithms under different settings of the UAV's transmit power and initial trajectory: (a) convergence analysis of Algorithm 1; (b) convergence analysis of Algorithm 2; (c) convergence analysis for Algorithm 3.

the four baseline schemes, which are called backscatter-assisted UAV-MEC, wireless-powered UAV-MEC, the complete offloading scheme, and the fully local computing scheme, respectively. For backscatter-assisted UAV-MEC or wireless-powered UAV-MEC, each IoT node only chooses BackCom or AT to offload tasks when it performs task offloading. In the complete offloading scheme, all IoT nodes' tasks are offloaded to the MEC server via BackCom, AT or hybrid passive and ACs, while in the fully local computing scheme, all IoT nodes' tasks are executed locally. Note that the above four schemes can also be obtained by using the proposed algorithms after making a few changes. Specifically, the backscatter-assisted UAV-MEC or the wireless-powered UAV-MEC is achieved by using the proposed algorithms with $p_k = 0$ and $t_k^a = 0 \ \ \forall k$ or $t_{n,k}^b = 0$ and $\alpha_{n,k} = 0 \ \ \forall n \ \ \forall k$, respectively. The complete offloading scheme is obtained by the proposed algorithms with $f_k = 0 \ \ \forall k$, while the fully local computing scheme is obtained via the proposed algorithms with $p_k = 0, t_k^a = 0, t_{n,k}^b = 0$, and $\alpha_{n,k} = 0 \ \ \forall n \ \ \forall k$.

Fig. 2 illustrates the convergence analysis of the proposed Algorithms 1–3 under different settings of the UAV's transmit power P_u and initial trajectory. Here, P_u is set as 0.5 and 1 W, respectively, and two initial trajectories are considered. For the first initial trajectory (denoted as "Initial trajectory 1"), the UAV flies straight with a constant speed from the initial position to the final position. For the second initial trajectory (denoted as "Initial trajectory 2"), the UAV is dispatched from its initial horizontal position [0, 0], flies straight to the position [5, 10], and then flies to its final horizontal position [10, 0] with a constant speed. Specifically, Fig. 2(a) is given to verify the convergence of Algorithm 1, where the communication resource allocation is determined by solving $\mathbf{P}_{3\mathrm{a}}$ with the given initial trajectory via CVX. Fig. 2(b) shows the convergence of Algorithm 2. In Fig. 2(c), the convergence of Algorithm 3 is demonstrated.

From Fig. 2(a), it can be seen that the proposed successive trajectory optimization algorithm in Algorithm 1 always converges to the optimal trajectory within three iterations, which verifies the effectiveness of Algorithm 1 and illustrates that Algorithm 1 has a fast convergence rate. The proposed two-stage alternating iterative algorithm in Algorithm 2 is provided to obtain the proposed scheme under the partial offloading mode. It can be observed from Fig. 2(b) that less than five iterations are required for Algorithm 2 to achieve a convergent state. This also indicates the effectiveness and fast convergence of Algorithm 2. Algorithm 3 provides the three-stage alternating iterative algorithm to achieve the proposed scheme under the binary offloading mode. From Fig. 2(c), we can see

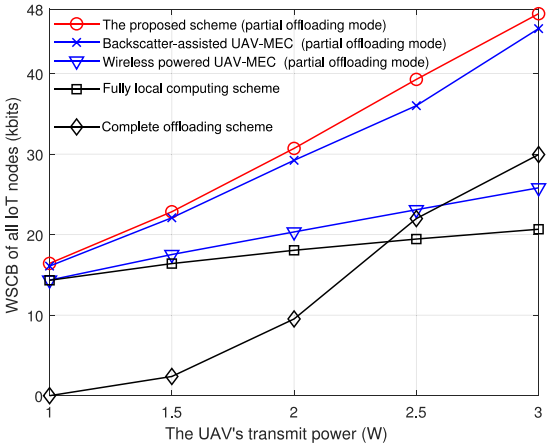

Fig. 3. WSCB of all IoT nodes under the partial offloading mode versus the UAV's transmit power.

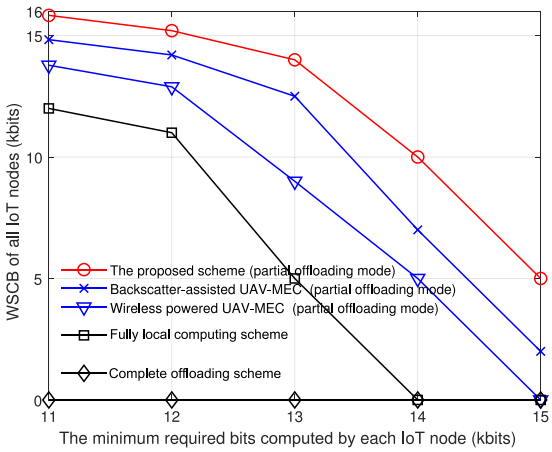

Fig. 4. WSCB of all IoT nodes under the partial offloading mode versus the minimum required bits computed by each IoT node.

that the proposed three-stage alternating iterative algorithm only needs several iterations (e.g., four iterations) to converge, which illustrates that Algorithm 3 is computationally effective with a fast convergence rate.

Fig. 3 plots the WSCB achieved by all IoT nodes versus P_u, where P_u ranges from 1 to 3 W and the partial offloading mode is considered for the investigated network. In order to show the advantage of the proposed scheme, the WSCB under the proposed scheme are compared with those obtained by the backscatter-assisted UAV-MEC, the wireless-powered UAV-MEC, the complete offloading scheme, and the fully local computing scheme. It can be observed from this figure that the WSCB achieved by all IoT nodes under all the schemes will increase when P_u increases. The reasons are as follows. When P_u is larger, the IoT nodes will offload more tasks to the MEC server via BackCom since the received RF signals are strong, and the total harvested energy per IoT node also increases, resulting in more tasks that can be offloaded by AT or executed locally. Thus, a larger P_u brings higher WSCB of all IoT nodes. By comparison, we can also find that the proposed scheme can achieve the best performance in terms of the WSCB of all IoT nodes among the above five schemes since the proposed scheme includes the superiorities of BackCom and AT, and can choose to offload how many task bits more flexibly compared with the complete offloading scheme and the fully local computing scheme. Besides, we can also see that the WSCB in the backscatter-assisted UAV-MEC is higher than those under the wireless-powered UAV-MEC since BackCom has a lower energy consumption for offloading task bits. Moreover, when P_u is large enough, the WSCB under the complete offloading scheme are higher than those under the fully local computing scheme, even higher than those obtained by the wireless-powered UAV-MEC. This is because a larger P_u brings a higher harvested energy per IoT node and then each IoT node has enough energy to support task offloading.

Fig. 4 plots the WSCB achieved by all IoT nodes versus the minimum required computation bits per IoT node, where the partial offloading mode is considered. Let $L_{\min,1} = L_{\min,2} = L_{\min,3} = L_{\min,4} = L_{\min}$ and then $L_{\min}$ ranges from 11 to 15 kbits. From this figure, we can see that with the increase of $L_{\min}$, the WSCB achieved by the proposed scheme, the backscatter-assisted UAV-MEC, the wireless-powered UAV-MEC and the fully local computing scheme will decrease, while the WSCB obtained by the complete offloading scheme is always 0. The reasons are listed below. A higher $L_{\min}$ indicates a more strict computation bits requirement for each IoT node. This will lead to a reduction to WSCB since in some cases, the IoT node may not satisfy this requirement. For the complete offloading scheme, P_u is not large enough to support all IoT nodes' task offloading while satisfying the minimum required computation bits. By comparison, it can also be seen that the proposed scheme outperforms the other schemes in terms of the WSCB of all IoT nodes, which also verifies the superiority of combining BackCom and AT.

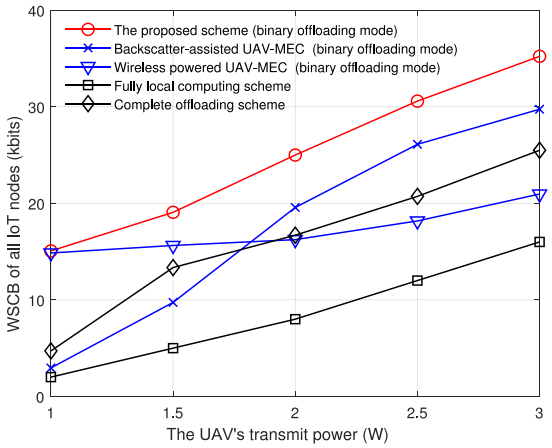

Fig. 5. WSCB of all IoT nodes under the binary offloading mode versus the UAV's transmit power.

Fig. 5 plots the WSCB achieved by all IoT nodes under the binary offloading mode versus P_u under different schemes, where $L_{\min} = 5$ kbits. We can observe that the WSCB of all IoT nodes under all the schemes increase with the increasing P_u and the proposed scheme is superior to the other schemes in terms of the WSCB of all IoT nodes since each IoT node can choose to perform either complete task offloading via BackCom, AT or hybrid passive and ACs, or fully local

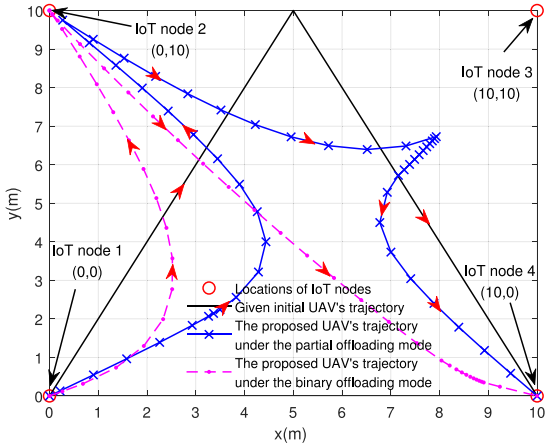

Fig. 6. UAV's trajectory under the partial and binary offloading modes.

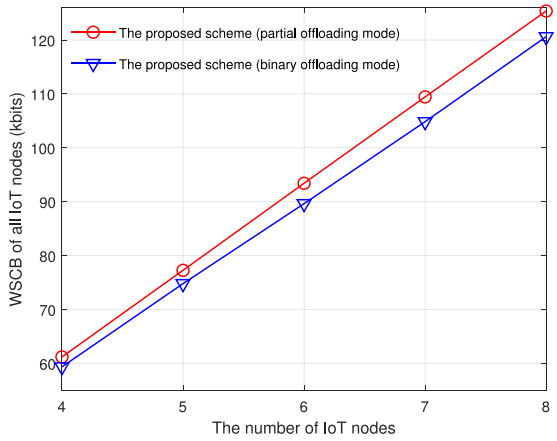

Fig. 7. WSCB of all IoT nodes under the partial and binary offloading modes versus the number of IoT nodes.

computing flexibly according to its channel gains, bringing an improvement to the computation performance.

Fig. 6 shows the UAV's trajectory under the partial and binary offloading modes. The black line denotes the given initial UAV's trajectory, the blue line with the mark of the blue cross represents the optimized trajectory of the UAV under the partial offloading mode achieved by applying Algorithm 2 while the pink dotted line with the mark of the pink dot expresses the optimized trajectory of the UAV under the binary offloading mode achieved by using Algorithm 3. The red circles denote the locations of all IoT nodes. As shown in this figure, the UAV is dispatched from its initial horizontal position $[0, 0]$ and then flies to its final horizontal position $[10, 0]$ at the end of the BackCom phase. It can be observed that the trajectory under the partial offloading mode is always close to IoT node 2 and IoT node 3 due to the fact that the weights of the two nodes are higher and the UAV needs to fly close to them to provide stronger RF signals for BackCom and more energy so that the WSCB of all IoT nodes can be improved. The trajectory under the binary offloading mode is close to IoT node 2 since its weight is highest. Different from the partial offloading mode, the trajectory under the binary offloading mode is not close to IoT 3 since in this case, only IoT 1 and IoT 2 choose to perform task offloading while the others compute their tasks locally. Therefore, there is no need for the UAV to fly close to IoT 3 to provide stronger RF signals for BackCom. By observations, we also find that the values of the weights can influence the UAV's trajectory and a proper weight can balance the performance of all IoT nodes.

Fig. 7 shows the WSCB of all IoT nodes under the partial and binary offloading modes versus the number of IoT nodes K, where $L_{\min} = 10$ kbits, K ranges from 4 to 8, and the weight of each IoT node is set as 1. It can be observed that the WSCB of all IoT nodes increase with K since with a larger K, more IoT nodes can compute and/or offload their tasks by using their received signals or harvested energy, bringing a higher WSCB. Besides, we also observe that the WSCB under the partial offloading mode is higher than that under the binary offloading mode. This is because the partial offloading mode is more flexible than the binary offloading mode, i.e., IoT nodes under the partial offloading mode can dynamically select the operation mode for achieving a higher WSCB according to the quality of the CSI.

VI. Conclusion

In this work, the resource allocation schemes for the partial and binary offloading modes were studied in a UAV-enabled WP-MEC network with hybrid passive and ACs. Specifically, two WSCB maximization problems were formulated by optimizing the local computation frequencies and time, the reflection coefficients, and the transmit powers of the IoT nodes, the UAV's trajectory, etc., subject to the QoS, energy causality, speed constraints, etc. Then, the optimization problem under the partial offloading mode was solved by the proposed two-stage alternating iterative algorithm, while a three-stage alternating iterative algorithm was proposed to solve the problem under the binary offloading mode. Computer results verified the effectiveness of the proposed algorithms and demonstrated the superiority of the proposed schemes under the partial and binary offloading modes over several baseline schemes in terms of WSCB.

Appendix A

In this section, Proposition 1 is proved by means of contradiction. Specifically, when other optimization variables, such as β, $\{t^b_{n,k}\}_{k=1}^K$, $\{t^a_k\}_{k=1}^K$, $\{p_k\}_{k=1}^K$, $\alpha_{n,k}$, and $\{f_i, \tau_i\}_{i=\{1,2,\ldots,K\}\backslash k}$, are given, f_k and τ_k should be jointly optimized to maximize the WSCB of all IoT nodes for the considered network. Let f_k^* and τ_k^* be the optimal computation frequency and time of the kth IoT node. Suppose that $\tau_k^* < T$ holds and both f_k^* and τ_k^* satisfy all the constraints of $\mathbf{P_{1a}}$. In this case, the maximum WSCB of all IoT nodes are computed as $R^*_{\text{total}} = \sum_{k=1}^K w_k(\sum_{n=1}^N t^b_{n,k} B\log_2(1 + [\xi\alpha_{n,k}P_u g_{n,k}h_k]/[B\sigma^2]) + t^a_k B\log_2(1 + [p_k h_k/B\sigma^2])) + \sum_{i=1,i\neq k}^K [w_i f_i \tau_i / C_{\text{cpu},i}] + [w_k f_k^* \tau_k^* / C_{\text{cpu},k}]$.

Then we construct another feasible solution, denoted by $\{f_k^+, \tau_k^+\}$, where $\tau_k^+ = T$ and $\tau_k^+ f_k^+ (f_k^+)^2 = \tau_k^* f_k^* (f_k^*)^2$. It can be observed that the constructed solution also satisfies all the constraints of $\mathbf{P_{1a}}$. Accordingly, the WSCB of all IoT nodes under the constructed solution can be computed as $R^+_{\text{total}} =$

$\sum_{k=1}^{K} w_k(\sum_{n=1}^{N} t_{n,k}^b B\log_2(1+[\xi\alpha_{n,k}P_u g_{n,k}h_k]/[B\sigma^2]) + t_k^a B\log_2(1+[p_k h_k/B\sigma^2])) + \sum_{i=1,i\neq k}^{K}([w_i f_i\tau_i]/[C_{\text{cpu},i}]) + ([w_k f_k^+\tau_k^+]/[C_{\text{cpu},k}])$. Since $\tau_k^+ = T > \tau^*$ and $\tau_k^+ f_k^+ (f_k^+)^2 = \tau_k^* f_k^* (f_k^*)^2$, we can obtain $f_k^+ < f_k^*$, leading to $\tau_k^+ f_k^+ > \tau_k^* f_k^*$. Then we have $R_{\text{total}}^+ > R_{\text{total}}^*$, which contradicts the above assumption. Therefore, the optimal computation time at the kth IoT node should be $\tau_k^* = T$.

APPENDIX B

As for $\mathbf{P}_{3a}$, C3, C4, C6-1, and C7-1 are linear constraints and whether $\mathbf{P}_{3a}$ is convex or not depends on the convexity-concavity of the objective function and constraints C1-2 and C2-2. That is, when the objective function is concave and both C1-2 and C2-2 are convex, $\mathbf{P}_{3a}$ is proved to be convex.

1) Concavity of the Objective Function: It can be observed that the objective function is concave if and only if function $f(x, y) = x\log_2(1+[y/x])$ is concave jointly regarding to x and y. Based on the fact that the perspective function can preserve convexity, it can be found that the convexity of $f(x, y)$ is the same as that of function $\log_2(1 + y)$ which is easily proved to be concave. Therefore, $f(x, y)$ is also a concave function, resulting in a concave objective function.

2) Convexities of Constraints C1-2 and C2-2: As for C1-2, its left side is a concave function and its right side is a constant. Thus, C1-2 is a convex constraint.

As for C2-2, its right side is a linear function while the convexity-concavity of its left side depends on that of function $f_1(x) = x^3$ with $x \geq 0$. Since $f_1(x) = x^3$ with $x \geq 0$ can be easily proved to be convex, C2-2 is also a convex constraint.

Based on the above analyses, $\mathbf{P}_{3a}$ can be proved to be convex.

APPENDIX C

Let $\boldsymbol{\theta} = (\theta_1, \theta_2, \ldots, \theta_K)$, $\boldsymbol{\varpi} = (\varpi_0, \varpi_1, \varpi_2, \ldots, \varpi_K)$, $\boldsymbol{\phi} = (\phi_1, \phi_2, \ldots, \phi_K)$, $\boldsymbol{\mu} = (\mu_0, \mu_1, \ldots, \mu_N)$, and $\boldsymbol{\varphi} = \begin{pmatrix} \varphi_{1,1} & \cdots & \varphi_{1,K} \\ \vdots & \ddots & \vdots \\ \varphi_{N,1} & \cdots & \varphi_{N,K} \end{pmatrix}$ express the nonnegative Lagrange multipliers regarding to all the constraints for $\mathbf{P}_{3a}$. Then the Lagrangian function of $\mathbf{P}_{3a}$ can be written as (17), shown at the bottom of the page.

On this basis, we can take the partial derivatives of $\mathcal{L}$ with respect to $x_{n,k}$ and P_k, as an effort to achieve the expressions for the optimal power reflection coefficient in the nth time slot and the optimal transmit power of the kth IoT node in closed forms, given by

$$\frac{\partial\mathcal{L}}{\partial x_{n,k}} = \frac{(w_k+\theta_k)\xi P_u g_{n,k}h_k B}{\left(B\sigma^2+\alpha_{n,k}\xi P_u g_{n,k}h_k\right)\ln 2} - \varpi_k P_u g_{n,k}\eta - \varphi_{n,k} \tag{18}$$

$$\frac{\partial\mathcal{L}}{\partial P_k} = \frac{(w_k+\theta_k)h_k B}{\left(B\sigma^2+p_k h_k\right)\ln 2} - \varpi_k. \tag{19}$$

By letting $(\partial\mathcal{L}/\partial x_{n,k}) = 0$, the optimal power reflection coefficient at the kth IoT node in the nth time slot $\alpha_{n,k}^*$ can be computed as follows:

$$\alpha_{n,k}^* = \left[\frac{(w_k+\theta_k)B}{\left(\varpi_k P_u g_{n,k}\eta+\varphi_{n,k}\right)\ln 2} - \frac{B\sigma^2}{\xi P_u g_{n,k}h_k}\right]^+ \quad \forall n \quad \forall k \tag{20}$$

where $[x]^+ = \max\{x, 0\}$. Similarly, by letting $(\partial\mathcal{L}/\partial P_k) = 0$, we can obtain the optimal transmit power at the kth IoT node p_k^* as

$$p_k^* = \left[\frac{(w_k+\theta_k)B}{\varpi_k\ln 2} - \frac{B\sigma^2}{h_k}\right]^+ \quad \forall k. \tag{21}$$

In order to achieve the closed-form expression of the optimal local computation frequency at the kth IoT node, we take the partial derivative of $\mathcal{L}$ regarding to f_k and obtain

$$\frac{\partial\mathcal{L}}{\partial f_k} = \frac{(w_k+\theta_k)T}{C_{\text{cpu},k}} - 3\varpi_k\varepsilon_k T f_k^2 - \phi_k. \tag{22}$$

Letting $(\partial\mathcal{L}/\partial f_k) = 0$, we can calculate the optimal local computing frequency at the kth IoT node f_k^* as follows:

$$f_k^* = \sqrt{\frac{(w_k+\theta_k)}{3\varpi_k\varepsilon_k C_{\text{cpu},k}} - \frac{\phi_k}{3\varpi_k\varepsilon_k T}} \quad \forall k. \tag{23}$$

Based on (20), (21), and (23), Theorem 1 can be obtained.

$$\begin{aligned}\mathcal{L} = &\sum_{k=1}^{K} w_k\left(\sum_{n=1}^{N} t_{n,k}^b B\log_2\left(1+\frac{\xi x_{n,k}P_u g_{n,k}h_k}{t_{n,k}^b B\sigma^2}\right) + t_k^a B\log_2\left(1+\frac{P_k h_k}{t_k^a B\sigma^2}\right) + \frac{f_k T}{C_{\text{cpu},k}}\right)\\ &+ \sum_{k=1}^{K}\theta_k\left(\sum_{n=1}^{N} t_{n,k}^b B\log_2\left(1+\frac{\xi x_{n,k}P_u g_{n,k}h_k}{t_{n,k}^b B\sigma^2}\right) + t_k^a B\log_2\left(1+\frac{P_k h_k}{t_k^a B\sigma^2}\right) + \frac{f_k T}{C_{\text{cpu},k}} - L_{\min,k}\right)\\ &+ \sum_{k=1}^{K}\varpi_k\left(\sum_{n=1}^{N}\left(\frac{\beta T}{N}P_u g_{n,k}\eta - x_{n,k}P_u g_{n,k}\eta\right) - \varepsilon_k(f_k)^3 T - P_{\text{c},k}\left(\sum_{n=1}^{N} t_{n,k}^b\right) - P_k - p_{\text{c},k}t_k^a\right)\\ &+ \sum_{k=1}^{K}\phi_k\left(f_k^{\max} - f_k\right) + \mu_0(1-\beta) + \sum_{n=1}^{N}\mu_n\left(\frac{\beta T}{N} - \sum_{k=1}^{K} t_{n,k}^b\right) + \varpi_0\left((1-\beta)T - \sum_{k=1}^{K} t_k^a\right)\\ &+ \sum_{k=1}^{K}\sum_{n=1}^{N}\varphi_{n,k}\left(t_{n,k}^b - x_{n,k}\right)\end{aligned} \tag{17}$$

REFERENCES

[1] J. Li, M. Dai, and Z. Su, "Energy-aware task offloading in the Internet of Things," *IEEE Wireless Commun.*, vol. 27, no. 5, pp. 112–117, Oct. 2020.

[2] C. R. Valenta and G. D. Durgin, "Harvesting wireless power: Survey of energy-harvester conversion efficiency in far-field, wireless power transfer systems," *IEEE Microw. Mag.*, vol. 15, no. 4, pp. 108–120, Jun. 2014.

[3] Y. Mao, C. You, J. Zhang, K. Huang, and K. B. Letaief, "A survey on mobile edge computing: The communication perspective," *IEEE Commun. Surveys Tuts.*, vol. 19, no. 4, pp. 2322–2358, 4th Quart., 2017.

[4] Y. Ye, R. Q. Hu, G. Lu, and L. Shi, "Enhance latency-constrained computation in MEC networks using uplink NOMA," *IEEE Trans. Commun.*, vol. 68, no. 4, pp. 2409–2425, Apr. 2020.

[5] C. You, K. Huang, and H. Chae, "Energy efficient mobile cloud computing powered by wireless energy transfer," *IEEE J. Sel. Areas Commun.*, vol. 34, no. 5, pp. 1757–1771, May 2016.

[6] L. Huang, S. Bi, and Y. J. Zhang, "Deep reinforcement learning for Online computation offloading in wireless powered mobile-edge computing networks," *IEEE Trans. Mobile Comput.*, vol. 19, no. 11, pp. 2581–2593, Nov. 2020.

[7] F. Wang, J. Xu, X. Wang, and S. Cui, "Joint offloading and computing optimization in wireless powered mobile-edge computing systems," *IEEE Trans. Wireless Commun.*, vol. 17, no. 3, pp. 1784–1797, Mar. 2018.

[8] S. Mao, S. Leng, K. Yang, X. Huang, and Q. Zhao, "Fair energy-efficient scheduling in wireless powered full-duplex mobile-edge computing systems," in *Proc. IEEE GLOBECOM*, 2017, pp. 1–6.

[9] L. Ji and S. Guo, "Energy-efficient cooperative resource allocation in wireless powered mobile edge computing," *IEEE Internet Things J.*, vol. 6, no. 3, pp. 4744–4754, Jun. 2019.

[10] L. Shi, Y. Ye, X. Chu, and G. Lu, "Computation energy efficiency Maximization for a NOMA-based WPT-MEC network," *IEEE Internet Things J.*, vol. 8, no. 13, pp. 10731–10744, Jul. 2021.

[11] F. Zhou, H. Sun, Z. Chu, and R. Q. Hu, "Computation efficiency Maximization for wireless-powered mobile edge computing," in *Proc. IEEE GLOBECOM*, 2018, pp. 1–6.

[12] Y. Ye, L. Shi, X. Chu, G. Lu, and S. Sun, "Mutualistic cooperative ambient backscatter communications under hardware impairments," *IEEE Trans. Commun.*, early access, Aug. 24, 2022, doi: 10.1109/TCOMM.2022.3201119.

[13] S. Gong, Y. Xie, J. Xu, D. Niyato, and Y.-C. Liang, "Deep reinforcement learning for backscatter-aided data offloading in mobile edge computing," *IEEE Netw.*, vol. 34, no. 5, pp. 106–113, Sep./Oct. 2020.

[14] Y. Zou, J. Xu, S. Gong, Y. Guo, D. Niyato, and W. Cheng, "Backscatter-aided hybrid data offloading for wireless powered edge sensor networks," in *Proc. IEEE GLOBECOM*, 2019, pp. 1–6.

[15] L. Shi, Y. Ye, G. Zheng, and G. Lu, "Computational EE fairness in backscatter-assisted wireless powered MEC networks," *IEEE Wireless Commun. Lett.*, vol. 10, no. 5, pp. 1088–1092, May 2021.

[16] Y. Ye, L. Shi, X. Chu, D. Li, and G. Lu, "Delay minimization in wireless powered mobile edge computing with hybrid BackCom and AT," *IEEE Wireless Commun. Lett.*, vol. 10, no. 7, pp. 1532–1536, Jul. 2021.

[17] J. Lu, P. Wu, and M. Xia, "Computation-efficient hybrid offloading for backscatter-assisted wirelessly powered MEC," in *Proc. IEEE VTC-Spring*, 2021, pp. 1–6.

[18] L. Shi, Y. Ye, X. Chu, and G. Lu, "Computation bits maximization in a backscatter assisted wirelessly powered MEC network," *IEEE Commun. Lett.*, vol. 25, no. 2, pp. 528–532, Feb. 2021.

[19] Y. Ye, L. Shi, X. Chu, R. Q. Hu, and G. Lu, "Resource allocation in backscatter-assisted wireless powered MEC networks with limited MEC computation capacity," *IEEE Trans. Wireless Commun.*, early access, Jun. 30, 2022, doi: 10.1109/TWC.2022.3185825.

[20] F. Cheng, G. Gui, N. Zhao, Y. Chen, J. Tang, and H. Sari, "UAV-relaying-assisted secure transmission with caching," *IEEE Trans. Commun.*, vol. 67, no. 5, pp. 3140–3153, May 2019.

[21] X. Pang, N. Zhao, J. Tang, C. Wu, D. Niyato, and K.-K. Wong, "IRS-assisted secure UAV transmission via joint trajectory and beamforming design," *IEEE Trans. Commun.*, vol. 70, no. 2, pp. 1140–1152, Feb. 2022.

[22] Y. Liu, K. Xiong, Q. Ni, P. Fan, and K. B. Letaief, "UAV-assisted wireless powered cooperative mobile edge computing: Joint offloading, CPU control, and trajectory optimization," *IEEE Internet Things J.*, vol. 7, no. 4, pp. 2777–2790, Apr. 2020.

[23] F. Zhou, Y. Wu, R. Q. Hu, and Y. Qian, "Computation rate maximization in UAV-enabled wireless-powered mobile-edge computing systems," *IEEE J. Sel. Areas Commun.*, vol. 36, no. 9, pp. 1927–1941, Sep. 2018.

[24] W. Feng et al., "Hybrid Beamforming design and resource allocation for UAV-aided wireless-powered mobile edge computing networks with NOMA," *IEEE J. Sel. Areas Commun.*, vol. 39, no. 11, pp. 3271–3286, Nov. 2021.

[25] X. Hu, K.-K. Wong, and Y. Zhang, "Wireless-powered edge computing with cooperative UAV: Task, time scheduling and trajectory design," *IEEE Trans. Wireless Commun.*, vol. 19, no. 12, pp. 8083–8098, Dec. 2020.

[26] Y. Du, K. Yang, K. Wang, G. Zhang, Y. Zhao, and D. Chen, "Joint resources and workflow scheduling in UAV-enabled wirelessly-powered MEC for IoT systems," *IEEE Trans. Veh. Technol.*, vol. 68, no. 10, pp. 10187–10200, Oct. 2019.

[27] D. Darsena, G. Gelli, and F. Verde, "Modeling and performance analysis of wireless networks with ambient backscatter devices," *IEEE Trans. Commun.*, vol. 65, no. 4, pp. 1797–1814, Apr. 2017.

[28] H. Yang, Y. Ye, X. Chu, and S. Sun, "Energy efficiency Maximization for UAV-enabled hybrid backscatter-harvest-then-transmit communications," *IEEE Trans. Wireless Commun.*, vol. 21, no. 5, pp. 2876–2891, May 2022.

[29] Y. Ye, L. Shi, X. Chu, and G. Lu, "Throughput fairness guarantee in wireless powered backscatter communications with HTT," *IEEE Wireless Commun. Lett.*, vol. 10, no. 3, pp. 449–453, Mar. 2021.

[30] L. Shi, Y. Ye, R. Q. Hu, and H. Zhang, "Energy efficiency Maximization for SWIPT enabled two-way DF relaying," *IEEE Signal Process. Lett.*, vol. 26, no. 5, pp. 755–759, May 2019.

[31] Y. Ye, L. Shi, X. Chu, and G. Lu, "On the outage performance of ambient backscatter communications," *IEEE Internet Things J.*, vol. 7, no. 8, pp. 7265–7278, Aug. 2020.

[32] H. Yang, Y. Ye, and X. Chu, "Max-min energy-efficient resource allocation for wireless powered backscatter networks," *IEEE Wireless Commun. Lett.*, vol. 9, no. 5, pp. 688–692, May 2020.

[33] L. Shi, R. Q. Hu, Y. Ye, and H. Zhang, "Modeling and performance analysis for ambient backscattering underlaying cellular networks," *IEEE Trans. Veh. Technol.*, vol. 69, no. 6, pp. 6563–6577, Jun. 2020.

[34] S. Boyd and L. Vandenberghe, *Convex Optimization*. Cambridge, U.K.: Cambridge Univ. Press, 2004.

[35] H. Zhang, C. Jiang, N. C. Beaulieu, X. Chu, X. Wen, and M. Tao, "Resource allocation in spectrum-sharing OFDMA femtocells with heterogeneous services," *IEEE Trans. Commun.*, vol. 62, no. 7, pp. 2366–2377, Jul. 2014.

Qian Li received the master's degree in computer application technology from Huazhong University of Science and Technology, Wuhan, China, in 2007.

Since July 2000, she has been a full-time Teacher with the School of Computer Science and Technology, Zhoukou Normal University, Zhoukou, China, and was promoted to associate professor in 2013. She is currently the Leader of Software Engineering major with Zhoukou Normal University. She is a member of the Agricultural Information Management Innovation Technology Team of colleges and universities in Henan Province. She has been supported by more than ten projects, including the Provincial Higher Education Teaching Reform Research and Practice Project, and the Provincial Science and Technology Department Science and Technology Research Project. Her research interests include Internet of Things security and artificial intelligence.

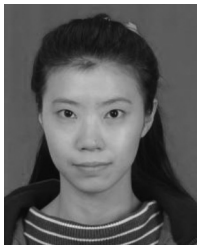

Liqin Shi received the B.S. degree from Sichuan University, Chengdu, China, in 2015, and the Ph.D. degree from Xidian University, Xi'an, China, in 2020.

She was a joint Ph.D. student with the Department of Electrical and Computer Engineering, Utah State University, Logan, Utah, from 2018 to 2019. In 2020, she joined Xi'an University of Posts and Telecommunications, Xi'an, where she is currently an Associate Professor with the Department of Communication and Information Engineering. She has published more than 20 papers in the IEEE transactions, journals, letters, and conferences. Her research interests include wireless energy harvesting and mobile edge computing.

Dr. Shi is also a Reviewer of multiple international journals, including the IEEE JOURNAL ON SELECTED AREAS IN COMMUNICATIONS and IEEE TRANSACTIONS ON WIRELESS COMMUNICATIONS.

Zhongjun Zhang received the M.S. degree in computer software and theory from Zhengzhou University, Zhengzhou, China, in 2009.

Since July 2009, he has been a full Teacher with the School of Computer Science and Technology, Zhoukou Normal University, Zhoukou, China. He is currently the Researcher with the Henan Engineering Laboratory of "Traceability Technology for Quality and Safety of Agricultural Products." He has been funded by over ten projects, including Science and Technology Research Project of Provincial Science and Technology Department and the Key Projects of Provincial Education Department. His research interests include data mining, artificial intelligence, and social networks.

Mr. Zhang was awarded by the First Prize of provincial education information achievements in 2016, and awarded excellent teachers for many times for his excellent contributions in education and research.

Gan Zheng (Fellow, IEEE) received the B.Eng. and M.Eng. degrees in electronic and information engineering from Tianjin University, Tianjin, China, in 2002 and 2004, respectively, and the Ph.D. degree in electrical and electronic engineering from The University of Hong Kong, Hong Kong, in 2008.

He is currently a Professor of Connected Systems with the School of Engineering, University of Warwick, Coventry, U.K. His research interests include machine learning for wireless communications, UAV communications, mobile edge caching, full-duplex radio, and wireless power transfer.

Prof. Zheng is the first recipient of the 2013 IEEE SIGNAL PROCESSING LETTERS Best Paper Award, and he also received the 2015 GLOBECOM Best Paper Award and the 2018 IEEE Technical Committee on Green Communications & Computing Best Paper Award. He was listed as a Highly Cited Researcher by Thomson Reuters/Clarivate Analytics in 2019. He currently serves as an Associate Editor for IEEE WIRELESS COMMUNICATIONS LETTERS.